Physics – Uspekhi **52** (8) 835 – 860 (2009)

CONFERENCES AND SYMPOSIA

PACS numbers: 01.10.Fv, **63.20. – e**, 68.35.Rh, **75.80. + q**, **77.55. + f**, **77.80. – e**

Magnetoelectricity
(Scientific session of the Physical Sciences Division of the Russian Academy of Sciences, 20 January 2009)

A A Gorbatsevich, O E Omel'yanovskii, V I Tsebro; A K Zvezdin, A P Pyatakov; A A Mukhin, V Yu Ivanov, V D Travkin, A S Prokhorov, A A Volkov, A V Pimenov, A M Shuvaev, A Loidl; V M Mukhortov, Yu I Golovko, Yu I Yuzyuk

DOI: 10.3367/UFNe.0179.200908g.0887

A scientific session of the Physical Sciences Division of the Russian Academy of Sciences (RAS) devoted to the problem of magnetoelectricity was held on 20 January 2009 in the conference hall of the P N Lebedev Physical Institute, RAS. The following reports were presented at the session:

(1) **Gorbatsevich A A** (St. Petersburg Physico-Technical Center for Research and Education, RAS, St. Petersburg), **Omel'yanovskii O E, Tsebro V I** (P N Lebedev Physical Institute, RAS) "Toroidal ordering in crystals and nanostructures";

(2) **Zvezdin A K** (A M Prokhorov Institute of General Physics, RAS, Moscow), **Pyatakov A P** (A M Prokhorov Institute of General Physics, RAS, Moscow; Physics Department, M V Lomonosov Moscow State University, Moscow) "Inhomogeneous magnetoelectric interaction in multiferroics and related new physical effects";

(3) **Mukhin A A, Ivanov V Yu, Travkin V D, Prokhorov A S, Volkov A A** (A M Prokhorov Institute of General Physics, RAS, Moscow), **Pimenov A V, Shuvaev A M** (University of Wuerzburg, Germany), **Loidl A** (University of Augsburg, Germany) "Terahertz spectroscopy and the magnetoelectric properties of manganite-based multiferroics";

(4) **Mukhortov V M, Golovko Yu I** (Southern Scientific Center, RAS, Rostov-on-Don), **Yuzyuk Yu I** (Physics Department, Southern Federal University, Rostov-on-Don) "Heteroepitaxial films of a bismuth ferrite multiferroic doped with neodymium".

An abridge version of the reports is given below.

PACS number: **77.80. – e**
DOI: 10.3367/UFNe.0179.200908h.0887

Toroidal ordering in crystals and nanostructures

A A Gorbatsevich, O E Omel'yanovskii, V I Tsebro

1. States with a broken symmetry are traditionally the focus of attention of the condensed state physics. The physical nature of a change in macroscopic symmetry is connected with the appearance of this or that type of ordering. The modern technologies of nano- and heterostructures provide the possibility of controlling not only the parameters of the energy spectra and wave functions, but also the macroscopic symmetry of a system. The physical manifestations of the violation of macroscopic symmetry in nanostructures can be more vividly pronounced than in bulk materials [1, 2]. Formally, the response of a system to external actions is determined by a set of matrix elements of the operators of physical quantities, whose structure, in turn, is governed by the macroscopic symmetry of the system. Nanostructures differ from the conventional bulk materials with an analogous symmetry because of the difference in the characteristic spatial scales of the variation of the potential energy determining the symmetry of a system. In bulk materials, this scale is on the level of interatomic distances. In nanostructures, this scale can be substantially larger, reaching the maximum characteristic dimension at which the concept of the wave function of charge carriers remains valid, i.e., the coherence length. Correspondingly, the characteristic scale of spatial changes in the wave functions of charge carriers in the nanostructures is substantially greater than in the bulk materials, and, as a result, the magnitudes of matrix elements determining both the equilibrium characteristics of the system and its response to external actions that disturb equilibrium also substantially exceed those in the bulk materials.

In nonmagnetic materials, the spatial symmetry is determined by the charge distribution. The symmetry of magnetic materials is connected with the ordering of microscopic magnetic moments and currents, which breaks the time-reversal invariance. The type of ordering in this case is characterized by an order parameter [3] whose symmetry corresponds to a change in the macroscopic symmetry of the system upon its transition into an ordered state (in the general case, the order parameter is a tensor which represents one of the irreducible representations of the symmetry group of the low-temperature phase).

Thus, for instance, in the case of a symmetry group formed by the operations of spatial and time inversion, which has four vector representations, four vector order parameters can exist [4, 5]: polar vector of electric polarization **P** invariant relative to the inversion of time t; axial t-odd vector of magnetic moment **M**; polar t-odd vector of the toroid moment **T** whose symmetry also coincides with the symmetry of the electric current **j** and vector potential **A**, and axial t-even vector **G** which characterizes the ordering of spin

Uspekhi Fizicheskikh Nauk **179** (8) 887 – 913 (2004)
DOI: 10.3367/UFNr.0179.200908g.0887
Translated by S N Gorin; edited by A Radzig

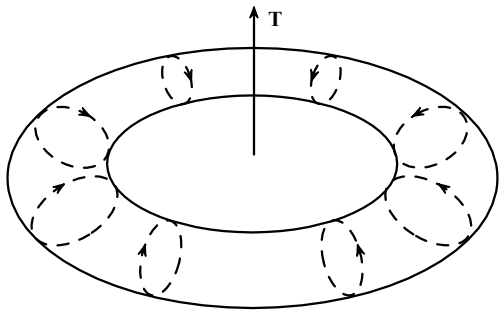

Figure 1. Geometrical image of a toroid moment.

currents in the system. The electric polarization **P** and the magnetization **M** play the role of the order parameters in ferroelectrics and in ferromagnets, respectively.

In the ordered state characterized by a vector **T**, a breakdown of both spatial and time symmetry takes place. This situation is possible in multiferroics — substances in which there coexist ferroelectric and magnetic ordering [6–10]. In multiferroics, the electric effects can substantially change the magnetic properties of the system, and the magnetic field changes the electrical properties, which accounts for the significant interest in these materials from the viewpoint of practical applications. However, the breakdown of both time and spatial symmetry can be connected not only with the presence of magnetic moments and electric polarization, but also with the existence of a nonzero spontaneous electric-current density in systems with toroidal ordering [11].

An object with the symmetry of a toroid moment (Fig. 1) was apparently introduced for the first time by Zel'dovich [12] when considering the phenomenon of parity violation. Parity nonconservation allows the existence of a pseudoscalar a which changes its sign upon coordinate inversion. Consequently, a particle which possesses spin **S** can also be described by a vector **T** related to spin **S** as follows:

$$\mathbf{T} = a\mathbf{S}\,.$$

Later on, a t-odd polar vector in crystals appeared in Ascher's works in connection with the consideration of the possibility of the existence of spontaneous currents [13] and kinetomagnetic and kinetoelectric effects [14], where 31 magnetic classes that allow the existence of this vector were defined. It is important, however, that by itself the electric current **j** cannot be considered as an order parameter, since this is forbidden by the requirement of the gauge invariance of the system energy [15, 16]. Indeed, if it is the current **j** that is chosen as the order parameter, then the Landau expansion for the free energy in a magnetic field H ($\mathbf{H} = \operatorname{rot}\mathbf{A}$), namely

$$F = aj^2 + bj^4 + \ldots - \frac{1}{c}\,\mathbf{jA}\,,$$

is obviously noninvariant relative to the gauge transformation $\mathbf{A} \to \mathbf{A} + \nabla\chi$, where $\chi(\mathbf{r}, t)$ is an arbitrary function.

In the classical theory of electromagnetism, the toroid moments appear as a third independent family (together with electric and magnetic moments) of electromagnetic multipoles [17, 18]. The toroid dipole moment appears in the same order of multipole expansion as the electric and magnetic quadrupoles [17–20]. The connection of the current density with the toroid dipole moment density has the form

$$\mathbf{j} = c\operatorname{rot}\operatorname{rot}\mathbf{T}\,, \tag{1}$$

and the total toroid moment of a volume element is expressed through the current density as follows:

$$\mathbf{T}_\Sigma = \frac{1}{10c}\int \left[\mathbf{r}\,(\mathbf{r}\,\mathbf{j}) - 2r^2\mathbf{j}\right] \mathrm{d}^3 r\,. \tag{2}$$

The role of the conjugate field (source) for the order parameter in the expansion of the free-energy density in the powers of the toroid moment density is played by the total current $\mathbf{J} = (c/4\pi)\operatorname{rot}\mathbf{B}$. In this case, since the symmetry of the toroid moment also coincides with the symmetry of the Poynting vector, the vector product [**EH**] can also serve as its source. Thus, the expansion of the free-energy density in a series in the powers of the toroid parameter in external fields takes the form

$$F = \alpha T^2 + \beta T^4 + \ldots - \gamma\mathbf{T}[\mathbf{EH}] - \mathbf{T}\operatorname{rot}\mathbf{B}\,, \tag{3}$$

where, as usual, $\alpha \propto (\theta - \theta_c)$, θ_c is the transition temperature, and α, β, and γ are the parameters of the material. The concept of the toroid moment as an order parameter was introduced in Refs [5, 11] (see also Refs [2, 21, 22]), and in Refs [23, 24] it was proposed to call substances with a nonzero density of toroid moment toroics.

A toroid moment can be connected with both the orbital currents and localized moments, including those of a purely spin nature. By substituting the expression for the current density written through the magnetization, namely

$$\mathbf{j} = c\operatorname{rot}\mathbf{M}\,,$$

into formula (2), we obtain

$$\mathbf{T}_\Sigma = \frac{1}{2}\int (\mathbf{r}\times\mathbf{M})\,\mathrm{d}^3 r\,,$$

which for the discrete moments goes over into the relationship

$$\mathbf{T}_\Sigma = \frac{1}{2}\sum_i \mathbf{r}_i \times \mathbf{M}_i\,. \tag{4}$$

The simplest configurations of magnetic moments that possess a nonzero toroid moment are displayed in Fig. 2a, b.

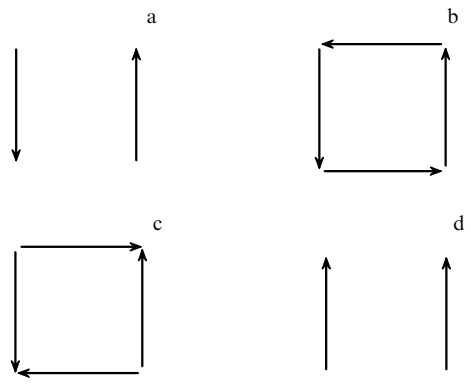

Figure 2. Simplest configurations of magnetic moments: (a, b) with a nonzero toroid moment, and (c, d) with a zero toroid moment (for an explanation, see the main text).

The configuration shown in Fig. 2a also possesses a quadrupole moment, whereas the configuration given in Fig. 2c has a quadrupole moment, but it does not have a toroid moment. Note that, as follows from Eqn (4), the definition of the toroid moment is single-valued and is independent of the choice of the origin under the condition that the total magnetic moment be equal to zero. However, even in the case of a nonzero magnetic moment, for example, in multiferroics, the concept of the toroid moment as an order parameter remains valid [20, 25]. The appearance of a toroid moment at the point of a phase transition in this case can be detected by calculating, according to formula (4), an increase in the toroid moment connected with an increase in magnetic moments. Indeed, for the toroid moment of a system of two magnetic moments M_1 and M_2 (Fig. 2d) oriented along the y-axis and located on the x-axis at the points x_1 and x_2, respectively $(x_2 = x_1 + d)$, we have

$$T_\Sigma = x_1 M_1 + x_2 M_2 = x_1(M_1 + M_2) + dM_2\,, \qquad (5)$$

i.e., the toroid moment obviously depends on the absolute value of x_1, which is connected with the choice of the origin. At $M_1 = M_2 = M_0$, the symmetry of the system does not allow the existence of a toroid moment. This can directly be checked by selecting the origin in the middle between the moments ($x_1 = -d/2$, $T_\Sigma = 0$). The transition into the toroid state occurs upon a change in the magnitudes of the magnetic moments corresponding to the configuration shown in Fig. 2d: $\delta M_{1,2} = \mp\delta M$. The change in the toroid moment, calculated from formula (5), no longer depends on the choice of the origin and coincides with the total toroid moment calculated with formula (5), when the 'correct' choice of the origin in the middle between the moments is made. In experiments, the appearance of a toroid moment can be detected by the appearance of an antisymmetric component of the magnetoelectric tensor $\alpha_{ik} - \alpha_{ki}$. It is precisely in this way that the appearance of a toroid moment was registered at the transition into the spin-flop phase in the strong magnetic field in Cr_2O_3 [26], and in the ferromagnetic compound $Ga_{2-x}Fe_xO_3$ [27]. A toroidal ordering was also revealed in a whole series of other compounds (see Ref. [25]), and recently toroidal domains have been identified by the optical method of the second harmonic generation in the compound $LiCoPO_4$ [28].

The thermodynamic properties of materials with a toroid moment are determined by expansion (3) and are independent of the nature of the toroid moment (spin or orbital), except for the magnitude of the coefficient γ, which characterizes the magnetoelectric effect in the expressions

$$\mathbf{M} = \gamma\,\mathbf{E} \times \mathbf{T}\,, \qquad \mathbf{P} = \gamma\,\mathbf{T} \times \mathbf{H}\,. \qquad (6)$$

In spin toroics, the magnitude of γ is determined by spin–orbit interaction and in the general case this coefficient is small. In the toroics of an orbital nature, this coefficient is determined by the Coulomb interaction and does not contain a spin-orbital smallness; therefore, the magnetoelectric effect can be great.

Figure 3 illustrates the physical mechanism of the appearance of a magnetoelectric effect in an orbital toroic. In the absence of external fields, the magnetic moments of the current contours located symmetrically relative to the toroid axis exactly compensate each other, and the total magnetic moment equals zero. The charge that creates

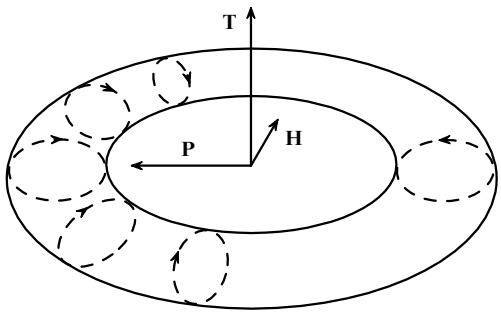

Figure 3. A schematic of the appearance of a magnetoelectric effect in an orbital toroic.

electric currents is also uniformly distributed over the surface of the toroid, and the electric polarization is absent. The external magnetic field orients the local current contours which form the toroid moment. The presence of a macroscopic toroidal symmetry at the microscopic level indicates the existence of a specific hardness of the construction of local currents, which limits their possible deformations. As can be seen from Fig. 3, the current contours are strung on the torus and a change in their orientation is unavoidably connected with a redistribution of the contours over the torus, which is accompanied by a redistribution of the charge and the appearance of electric polarization. On the other hand, the electric field, by transferring the charges, simultaneously moves the current contours over the surface of the toroid, which leads to the disturbance of the mutual compensation of the magnetic moments of elementary current contours and to the appearance of a total magnetic moment of the toroid.

According to formula (6), the toroid moment is dual to the antisymmetric component α_{ik} of the magnetoelectric tensor: $P_i = \alpha_{ik} H_k$, i.e., the toroics represent a subclass of magnetoelectrics [4, 7]. In a wider context, the toroics form a subclass of antiferromagnets. A fundamental difference of the toroics from other antiferromagnets is connected with the fact that the transition into the toroidal state is accompanied by the appearance of a singularity at the transition point of a new response function. This is the function of response to the current:

$$T_{\rm ind} = \chi_{\rm T} J\,, \qquad \chi_{\rm T} \sim \frac{1}{\theta - \theta_{\rm c}}\,,$$

where $\theta_{\rm c}$ is the transition temperature. This function can be measured by placing the specimen between the capacitor plates through which a displacement current is passed, namely

$$\mathbf{J} = \mathbf{J}_D = \frac{1}{4\pi}\frac{\partial \mathbf{D}}{\partial t}\,.$$

The presence of 'its own' conjugated field, whose role is played by the current, as well as of a special response function, explains the need to use, as the order parameter, precisely the density of toroid moment in those antiferromagnets where the symmetry allows its existence.

The special properties of toroics that are orbital in nature manifest themselves at the microscopic level. The presence in the system of a nonzero material t-odd polar vector $\mathbf{T}$, whose symmetry is analogous to the symmetry of the quasimomen-

tum, indicates the possibility of the existence of a linear-in-quasimomentum invariant in the expression for the energy:

$$\Delta E(\mathbf{k}) \propto \mathbf{T}\,\mathbf{k}\,. \tag{7}$$

Thus, the spectrum of elementary excitations in an orbital toroic is asymmetric in the quasimomentum [2, 16]. Depending on the magnitude of the spin–orbit interaction, the asymmetry of the spectrum must also be present in spin toroics, but the asymmetry in this case is small. It should be noted that the orbital antiferromagnetic ordering also appears in models of highly interacting particles [29], where it is known as a 'flux phase'.

The qualitative estimates made in Ref. [11] show that the orbital toroics can possess strong diamagnetism in the nonsuperconducting state (superdiamagnetism). The material magnetization M pertaining to the existence of a current contour with an area S and current J can be represented as $M = aJS$, where a is a certain constant. The paramagnetic component of the response to the external field, δM_S, in this case is related to a change in the area of the contour projection perpendicular to the direction of the magnetic field (i.e., to the orientation of the contour): $\delta M_S = aJ\,\delta S$. The diamagnetic component of the response is determined by a change in the current traversing the contour: $\delta M_J = aS\,\delta J$. When the magnetization serves as the order parameter Δ and the current density $\mathbf{j} = c\,\mathrm{rot}\,\mathbf{M}$, we can write for the total current $J \sim \Delta/\rho$, where ρ is the characteristic dimension of the contour projection ($S \sim \rho^2$). Consequently, $\delta M_J \sim -a\Delta\,\delta\rho$, $\delta M_S \sim 2a\Delta\,\delta\rho$, and the total change in the magnetization $\delta M = \delta M_S + \delta M_J \sim a\Delta\,\delta\rho$ proves to be of the same sign as that of δM_S, i.e., the response of the contour with current has a paramagnetic nature.

If the role of the order parameter is played by the toroid moment density, then the current defined by Eqn (1) is $J \sim \Delta/\rho^2$, and the diamagnetic and paramagnetic components of the response exactly compensate for each other. However, in the case of a spatially inhomogeneous system, there are grounds to expect that the total response will be diamagnetic, since the inhomogeneity can prevent a change in the orientation of the contour with current, thereby suppressing the paramagnetic component of the response.

The microscopic theory of superdiamagnetism [16] in spatially inhomogeneous toroics is based on the analogy between the toroidal order parameter and the vector potential. An essential difference between the toroidal order parameter and the usual vector potential is connected with the fact that the uniform vector potential does not have a physical sense and can be eliminated by a uniform shift in the momentum space (by a gauge transformation), whereas the asymmetry of the spectrum with respect to the quasimomentum in orbital toroics cannot be eliminated by any transformation, and it can lead to the observed physical effects.

In a toroic with a spatially inhomogeneous orbital order parameter, an effective pseudomagnetic field $\mathbf{B}_{\mathrm{eff}} = 4\pi\,\mathrm{rot}\,\mathbf{T}$ can be introduced. The toroidal order parameter in this case plays the role of an effective vector potential. The pseudomagnetic field renders on the charge carriers an action analogous to that of a usual magnetic field. The magnitude of the pseudomagnetic field, which is determined by the nature of toroidal ordering, can be very large in toroics orbital in nature. Correspondingly, the susceptibility χ of the system with respect to the true field B is determined by the differential susceptibility in the total field $B_{\mathrm{tot}} = B_{\mathrm{eff}} + B$:

$$\chi = -\left.\frac{\partial^2 F(B_{\mathrm{tot}})}{\partial B^2}\right|_{B=0}.$$

As is well known [30], the differential susceptibility in strong magnetic fields can be negative and large in magnitude, which is manifested, in particular, in the existence of diamagnetic domains [30, 31]. In the case of a spatially inhomogeneous toroic, the differential susceptibility in a strong pseudomagnetic field is nothing but the response of the system to a weak external magnetic field and, consequently, this response can be strongly diamagnetic.

Pseudomagnetic fields appear also in the description (in the mean-field approximation) of multiparticle effects in models of the quantum Hall effect [32, 33], of superfluid He^3-A [34], and of high-temperature superconductivity with the violation of t invariance [35, 36]. Recently, on the basis of the analogy between the density of the toroid moment and the vector potential, it was shown [37] that in the region of a domain boundary in a multiferroic a pseudomagnetic field appears, which establishes a force that is analogous to the Lorentz force, but acts on light, which explains the mechanism of the optical magnetoelectric effect [38].

The asymmetry of the spectrum in the quasimomentum means that the group velocities of carriers, $V(k) = (1/\hbar)\,\mathrm{d}E(k)/\mathrm{d}k$, with quasimomenta that are equal in magnitude and opposite in direction no longer compensate for each other as in ordinary materials. In this case, the total macroscopic current under equilibrium conditions becomes zero upon integration over the occupied states with the equilibrium distribution function $f_0(k) \equiv f_0(E(k))$, since the integrand is reduced to the total derivative:

$$\mathbf{j} = -2e\int \mathbf{V}(\mathbf{k})\,f(\mathbf{k})\,\frac{\mathrm{d}^3k}{(2\pi)^3} = \frac{2e}{\hbar}\int \frac{\mathrm{d}E(\mathbf{k})}{\mathrm{d}\mathbf{k}}\,f_0\bigl(E(\mathbf{k})\bigr)\,\frac{\mathrm{d}^3k}{(2\pi)^3}$$
$$= \int \frac{\mathrm{d}}{\mathrm{d}\mathbf{k}}\,(\ldots)\,\frac{\mathrm{d}^3k}{(2\pi)^3} \equiv 0\,. \tag{8}$$

However, under nonequilibrium conditions, if the nonequilibrium distribution function is not reduced to a function that depends only on the energy, $f(\mathbf{k}) \neq f(E(\mathbf{k}))$ (i.e., in particular, it does not possess a quasi-Fermi form), the integrand in formula (8) is no longer reduced to the total derivative and in the system there appears a macroscopic current

$$\mathbf{j} = \eta\,\mathbf{T}\,, \tag{9}$$

where η is a dissipative constant. Current (9) constitutes a current flowing in a nonequilibrium system in the absence of a gradient of electrochemical potential. The appearance of such a current is known as the anomalous photogalvanic effect (APGE) [39, 40]. Earlier, APGEs were described in systems without a center of inversion, which were connected with the asymmetry of charge-carrier scattering upon intraband collisions and/or interband transitions [39–42]. The velocity of carriers in this case is an odd function of quasimomentum, and the macroscopic APGE current appears due to an antisymmetric additive to the distribution function in the second order in the variable field. For describing this additive to the distribution function when solving the kinetic equation (or the equation for the density matrix) it is necessary to go beyond the framework of the Born approximation [39].

In bulk materials, states with a nontrivial symmetry are realized, as a rule, as a result of complex interparticle correlations and require the imposition of sufficiently rigorous restrictions on the parameters of interparticle interactions. In nanostructures, a state with an assigned spatial symmetry can be formed using traditional methods of engineering of wave functions, and the violation of invariance with respect to time inversion can be imitated by the action of an external magnetic field. Thus, it has been shown in Ref. [43] that a spectrum asymmetric in momentum, which is characteristic of systems with a toroidal type of ordering, is formed in asymmetric nanostructures (tunnel-coupled asymmetric quantum wells) in a magnetic field **H** parallel to the layers. The presence in this system of a material vector **T** with a symmetry of the toroid moment, which determines the asymmetry of the spectrum with respect to the quasimomentum, directly follows from symmetry considerations:

$$\mathbf{T} \propto \mathbf{l} \times \mathbf{H}, \tag{10}$$

where **l** is the polar vector directed along the axis of growth of quantum wells.

As to the electric polarization

$$\mathbf{P} \propto \mathbf{T} \times \mathbf{H} \tag{11}$$

in the magnetoelectric effect (MEE), it follows from formulas (10) and (11) that two types of MEEs nonlinear in the magnetic field should exist, namely, so-called longitudinal and transverse magnetoelectric effects. In the case of the longitudinal (with respect to the growth direction, i.e., to the asymmetry vector **l**) effect, the electric polarization changes in weak magnetic fields quadratically in the field strength:

$$P_x = \alpha_{\parallel} H_z^2, \tag{12}$$

where $\mathbf{l} \parallel x$, and $\alpha_{\parallel}$ is a proportionality factor depending on the degree of departure from equilibrium. Notice that, because of the symmetry of the system and the presence in it of a polar axis **l**, there is a certain polarization $\mathbf{P}_0 \propto \mathbf{l}$ even in the absence of external fields. The longitudinal magnetoelectric effect represents an addition to $\mathbf{P}_0$ related to the deformation of the wave functions of charge carriers in the magnetic field.

Of greater interest is the transverse magnetoelectric effect, in which case the plane of a heterostructure is inclined relative to the direction of the magnetic field in such a manner that one component of the magnetic field, H_z (which forms the toroid moment), is directed along the plane of quantum wells, and another, H_x (which causes a redistribution of current orbits in the toroidal configuration), is oriented along the asymmetry vector **l** of the heterostructure. In this case, an electric polarization arises in the lateral direction of the heterostructure along the plane of the quantum wells:

$$P_z = \alpha_{\perp} H_z H_x \propto H^2 \sin\varphi \cos\varphi \tag{13}$$

(here, φ is the inclination of the plane of the heterostructure relative to the direction of the magnetic field, and $\alpha_{\perp}$ is the corresponding proportionality factor), which occurs already on a scale of the lateral dimensions of the heterostructure, which in practice corresponds to dimensions on the order of several millimeters (but can also correspond to substantially greater sizes). Therefore, the transverse MEE, in contrast to the longitudinal effect, can easily be observed, and the preparation of specimens in this case does not require the application of lithography to creating the potential contacts, because it suffices to have two alloyed metallic contacts of arbitrary size and shape, spaced apart on the plane.

In the case where the breakdown of the symmetry relative to time inversion is caused by an external magnetic field, it is of interest to study the nonequilibrium properties, for the observation of which it is fundamentally important that the spectrum of elementary excitations be asymmetric.

2. The photogalvanic effect (PGE) and the magnetoelectric effect (MEE) were measured by our team both on undoped asymmetric heterostructures, in which no equilibrium charge carriers exist, and on doped structures with a finite density of equilibrium carriers. In both cases, we always used the photoexcitation of nonequilibrium carriers from the valence band by illuminating the heterostructure with light consisting of photons with the energies greater than the energy gap width (band–band transitions). In the case of PGE, the strength of the spontaneous current, according to formula (9), is determined by the degree of departure from equilibrium of the entire electron system and in doped structures with a significant number density of equilibrium carriers proves to be substantially less (as experiments showed, by many orders of magnitude) than in undoped structures.

As to the MEE, its appearance is primordially in no way caused by the nonequilibrium behavior of charge carriers and is a consequence, as was said above, of a redistribution of current trajectories of the orbital motion of charge carriers, which are responsible for the toroid moment, simultaneously with which there occurs a redistribution of the charge itself in the transverse or longitudinal (with respect to the asymmetry vector) direction. However, in this case as well, as was noted in Ref. [43], the magnitude of the electric polarization is very sensitive to the degree of departure from the system equilibrium, since the expression for the electric dipole moment in the first approximation contains the total derivative of energy with respect to the quasimomentum and vanishes when summing over occupied states with an equilibrium distribution function. According to paper [43], with switching-on dissipation, for instance, by using optical excitation, we should expect a sharp increase in electric polarization. As to the equilibrium polarization, it, in the limit of a strong magnetic field, should arise only in higher orders of magnitude in the holding potential [43].

It should be noted, however, that it is impossible to observe equilibrium polarization in a system with free equilibrium carriers, i.e., in a metallic system, such as a doped heterostructure, since under equilibrium conditions the electric field inside a metallic system should be zero. In our case this means that the redistribution of charge carriers caused by factors that are responsible for the magnetoelectric effect is completely compensated by free carriers in such a manner that a uniform charge distribution would be established over the entire volume. Thus, it occurs that, for doped (metallic) asymmetric heterostructures as well, the observation of a magnetoelectric effect is possible only under nonequilibrium conditions, i.e., in our case, upon optical excitation of charge carriers.

Samples of asymmetric heterostructures investigated, the scheme of measurements, and the geometry of experiments on the photogalvanic and magnetoelectric effects. Experiments on

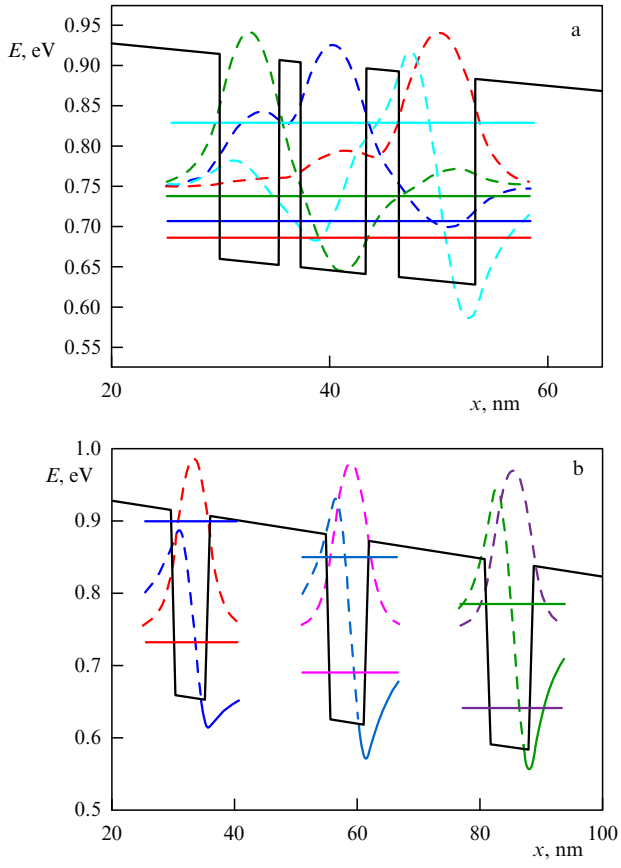

Figure 4. Energy profiles of two asymmetric undoped three-well $Al_xGa_{1-x}As/GaAs$ ($x = 0.25$) heterostructures with (a) tunnel-coupled (S1) and (b) separated (S1a) quantum wells. Levels of the size quantization and corresponding electron wave functions are shown.

Table 1. Layer-by-layer arrangement of two asymmetric undoped three-well $Al_xGa_{1-x}As/GaAs$ ($x = 0.25$) heterostructures with tunnel-coupled (S1) and separated (S1a) quantum wells.

Layer composition	Layer thickness, Å		Comment
	S1	S1a	
GaAs	100	100	Protective layer
$Al_xGa_{1-x}As$	200	200	
GaAs	54	54	Quantum well
$Al_xGa_{1-x}As$	20	200	Barrier
GaAs	60	60	Quantum well
$Al_xGa_{1-x}As$	30	200	Barrier
GaAs	70	70	Quantum well
$Al_xGa_{1-x}As$	200	200	
GaAs	5000	5000	Buffer layer

the observation of photogalvanic and magnetoelectric effects were performed on asymmetric (with respect to the growth direction) heterostructures of GaAs/AlGaAs and AlGaAs/InGaAs/GaAs systems grown by the molecular beam epitaxy (MBE) method. The following samples were investigated.

(a) Asymmetric undoped $Al_xGa_{1-x}As/GaAs$ ($x = 0.1-0.25$) structures with three quantum wells separated by thin transparent barrier layers; such a structure represents a single two-dimensional electron system with a width of about 250–350 Å and with several levels of size quantization. A layer-by-layer arrangement of one such heterostructure (S1) is illustrated in Table 1 and its energy profile, levels of size quantization, and appropriate electron wave functions are shown in Fig. 4a.

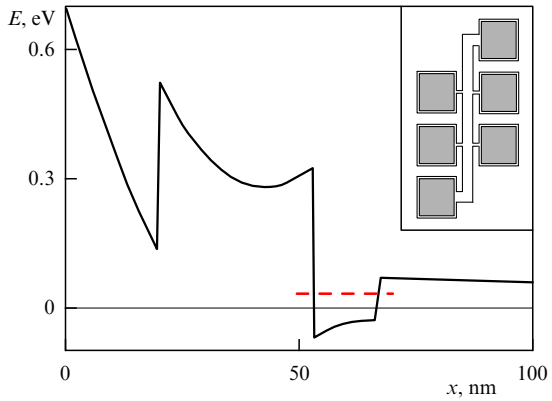

Figure 5. Energy profile of an asymmetric doped S512 heterostructure of $Al_xGa_{1-x}As/In_xGa_{1-x}As/GaAs$ system with a single level of size quantization (dashed line). In the inset to the figure is shown a planar form of the heterostructure samples prepared using lithography, with metallized bonding pads (for explanations, see the main text).

Table 2. Structure of an asymmetric doped heterostructure (S512) representing a single quantum well located between two barriers significantly differing in height (see Fig. 5).

Layer composition	Layer thickness, Å	x	Silicon concentration	Comment
GaAs	200		3×10^{17} cm^{-3}	Protective layer
$Al_xGa_{1-x}As$	300	0.28	7×10^{17} cm^{-3}	Doped region
$Al_xGa_{1-x}As$	30	0.28		Spacer
$In_xGa_{1-x}As$	135	0.2		Quantum well
GaAs	4300			Buffer layer

(b) Asymmetric undoped $Al_xGa_{1-x}As/GaAs$ ($x = 0.1-0.25$) structures with three quantum wells separated by thick barriers that are impenetrable to electrons, so that the three two-dimensional electronic layers are independent of each other (see data for the structure S1a in Table 1 and in Fig. 4b).

(c) Asymmetric doped heterostructure (S512) which represents a single quantum well $In_xGa_{1-x}As$ ($x = 0.2$) with a width of 135 Å between barriers of $Al_xGa_{1-x}As$ ($x = 0.28$) and GaAs that differ significantly in height. The layer-by-layer arrangement of this heterostructure is given in Table 2 and its energy profile is displayed in Fig. 5. In this quantum well, there is one level of size quantization below the Fermi level. Due to silicon doping of the region of the outer barrier lying behind the spacer, equilibrium charge carriers exist in the system, whose two-dimensional density at room temperature is 1.2×10^{12} cm^{-2} (0.78×10^{12} cm^{-2} at $T = 4.2$ K).

Samples of the undoped S1 and S1a heterostructures rectangular in shape (with dimensions of approximately 8×2 mm) each had two alloyed metallic (indium) potential contacts symmetrically located opposite each other at a distance of several millimeters (Figs 6c and 6d). The samples of the doped structure S512, which were prepared with the aid of lithography, had a so-called spider form (see inset to Fig. 5) intended for the measurement of transport properties, and in the plan view they represented a narrow strip 57 μm wide, on which metallized regions of potential contacts that were connected by even narrower (10 μm) bridges located at a distance of 0.27 mm from each other were applied. The

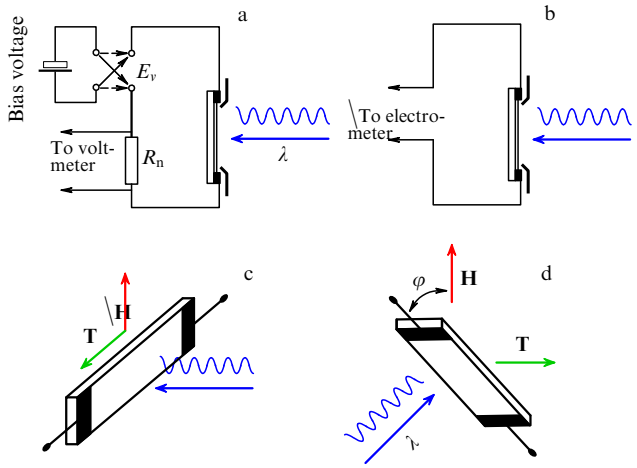

Figure 6. Geometry of experiments as well as the scheme of measurements of PGE and the longitudinal MEE (a, c), and the transverse MEE (b, d). Mutual orientations of the directions of the magnetic field and toroid moment relative to the plane of the heterostructure are shown.

overall length of the sample together with the bonding pads was 1.1 mm.

Measurements of the PGE and MEE were conducted in a special insert with an optical lead-in, placed vertically into a Dewar-vessel insert in a superconducting solenoid for measurements at intermediate temperatures. Light from a halogen lamp or a blue light emitting diode was put into the sample via a flexible light guide. The power of the supplied radiation was 5 mW at most; the radiation power density on the illuminated surface of the sample was approximately 0.35 mW mm^{-2}. The contacts and the adjacent regions of the sample were shut with a special protective shield. When measuring the PGE and the longitudinal MEE, the planes of the sample heterostructure layers were oriented along the magnetic field in such a manner that the line of the potential contacts of the samples was perpendicular to the field direction (Fig. 6c). In the measurements of the transverse MEE, the line of the potential contacts of the samples was oriented at an angle to the direction of the magnetic field in such a manner that the line of contacts, the asymmetry vector of the structure, and the magnetic field vector were located in one plane (Fig. 6d).

The electric circuit for measuring the PGE and the MEE was quite simple. Electric polarization in the magnetoelectric effect was measured on the potential contacts by a voltmeter with a very high input resistance or by an electrometer (Fig. 6b). As far as the PGE is concerned, initially the PGE current was measured in a simple closed series circuit consisting of the sample and a standard measuring resistance (Fig. 6a) [44]. In this case, the current determined from the voltage drop across the measuring resistance is the short-circuit current, since the resistance of the samples even under maximum illumination is considerably greater than the measuring resistance. It was possible, if necessary, to include an additional source of voltage in the metering circuit. Under these conditions, for example, we studied the magnetoresistance of an asymmetric heterostructure in the case of photoinduced charge carriers [45] and measured the current–voltage characteristics of the samples [44]. Notice that the alloying of a metallic (in our case, indium) contact to a certain depth is accompanied by the appearance of a potential barrier near the quantum well, which results in the appearance of a region depleted of charge carriers under the contact and in its immediate vicinity. This depleted near-contact region has a very high resistance, especially at low temperatures. Furthermore, at low temperatures the current–voltage characteristic of the contact/heterostructure/contact system becomes strongly nonlinear owing to the nonlinear properties of the near-contact regions, which considerably distorts the measured field dependences $J_{\rm PGE}(H)$ [44]. Therefore, we further measured the PGE, just as the MEE, almost always in a broken circuit from the potential difference $U_{\rm PGE}$ across the contacts to the heterostructure with the aid of an electrometer or a voltmeter with a very high input resistance. In this case, the effect of near-contact regions was eliminated completely and, if necessary, the photogalvanic current $J_{\rm PGE}$ was determined from the measured potential drop $U_{\rm PGE}$ and the known magnitude of the electrical resistance of the heterostructure at a given level of light excitation of charge carriers.

Photogalvanic effect in a strong magnetic field. The first experimental evidence for the existence of a sufficiently strong PGE in asymmetric heterostructures corresponding to the theoretical predictions of Ref. [43] can be considered to be the work by Aleshchenko et al. [46]. The authors of Ref. [46] detected a shift in the current–voltage curves of a three-well asymmetric $Al_xGa_{1-x}As/GaAs$ ($x = 0.25$) heterostructure depending on the direction of a DC 5-kOe magnetic field by a certain magnitude (varying with temperature) $V_{\rm PGE}$ (~ 0.25 V at $T \approx 300$ K), which was called by the authors the PGE emf. It was understandable that it was of interest to investigate the PGE in detail in a wide range of magnetic fields and temperatures using heterostructures with various asymmetric profiles, and this was performed in our subsequent work, beginning with Ref. [44].

Figure 7 displays the results of measurements of the field dependences of the potential difference, $U_{\rm PGE}(H)$, on various samples of undoped three-well $Al_xGa_{1-x}As/GaAs$ ($x = 0.25$) heterostructures in magnetic fields of up to 140 kOe at various temperatures and intensities of illumination with a halogen lamp. It is seen from the data given in Figs 7a and 7b for the heterostructure S1 that in all the cases the $U_{\rm PGE}(H)$ dependences represent H-odd functions that are linear in weak fields and are nonmonotonic (with well pronounced extrema) in strong fields. Worthy of mention are the large values of $U_{\rm PGE}$, which reach at the maximum (at $H \approx 20$ kOe), depending on the temperature and illumination conditions, 2–8 V per cm of length of the illuminated region of the heterostructure. At room temperature, with allowance for the measured electrical resistance (≈ 150 MΩ), this corresponds to a photogalvanic current $J_{\rm PGE}^{\rm max} \approx 10$ nA, which coincides with the data obtained in the short-circuit regime [44].

A linear increase in $U_{\rm PGE}$ at small H is a direct consequence of relations (9) and (10), i.e., of the fact that the magnitude of the toroid moment is linear in H in weak magnetic fields. With an increase in the magnetic field, $U_{\rm PGE}$ passes through a maximum and then decreases noticeably. It is understandable from general considerations that, as the magnetic length $L_H = (\hbar c/eH)^{1/2}$ becomes, with increasing H, less than the dimension of the three-well quantum region of the heterostructure along the asymmetry vector, processes of magnetic localization begin to manifest themselves; as a result, the shape of the potential that holds the carriers affects their behavior to a much less extent. Thus, the magnitude of

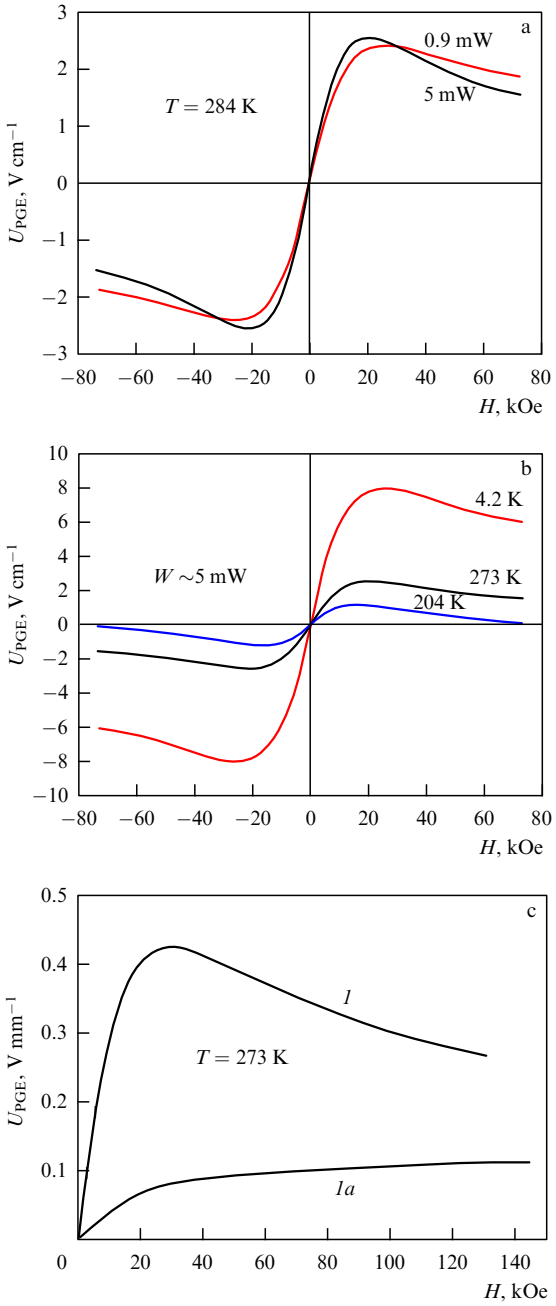

Figure 7. Field dependences $U_{PGE}(H)$ of the photogalvanic effect obtained on samples of asymmetric three-well undoped $Al_xGa_{1-x}As/GaAs$ ($x = 0.25$) heterostructures: (a) for the structure S1 at room temperature and illumination powers $W = 5$ and 0.9 mW; (b) for the structure S1 at $W = 5$ mW and $T = 273$, 204, and 4.2 K, and (c) for heterostructures with different tunnel coupling (curves *1* and *1a* refer to the structures S1 and S1a, respectively; see Table 1). The values of U_{PGE} are given in volts per unit length of the illuminated section of the heterostructure.

the asymmetry vector in formula (10) decreases in the range of strong fields with an increase in strength, and the toroid moment decreases correspondingly. The results of numerical calculations performed for the three-well heterostructure S1 in Ref. [45] show that with increasing H the electrons almost completely leave the two narrow quantum wells and are localized in the widest well. This leads not only to a strong decrease in the magnitude of the toroid moment, but also quite substantially affects the magnitude of the magnetoresistance when the photoinduced carriers are moving in the lateral plane of the heterostructure [$\Delta R(H)/R(0) = 1.85$ in a field of 75 kOe) [45], which in turn leads to a stronger field dependence of the photogalvanic current $J_{PGE}(H)$ as compared with $U_{PGE}(H)$ [44].

A comparison of the experimental data on the PGE, obtained in heterostructures with tunnel-coupled (S1) and separated (S1a) quantum wells gives evidence that the effect is much weaker in the samples with separated quantum wells (cf. curves *1* and *1a* in Fig. 7c) and in the field dependences of the PGE there is no maximum. The observed strong decrease in the PGE in the structures with narrow quantum wells separated by wide barrier layers impenetrable to electrons can be explained by the fact that in this case the toroidal states of the carriers are formed independently of each other in each quantum well whose potential energy profile and corresponding electron wave functions are much less asymmetric (Fig. 4b). As a consequence, the integral magnitude of the toroid moment induced by the magnetic field in each quantum well and in the entire structure on the whole proves to be considerably less than the one that could exist in the case of tunnel coupling between the quantum wells composing the structure. It is also understandable that the magnetic localization in this case must show itself only in very strong fields ($\sim$ 500 kOe), which explains the absence of a maximum in the PGE field dependences.

Transverse magnetoelectric effect in the undoped heterostructures of the AlGaAs/GaAs system. The results of measurements of the field dependences of electric polarization in circumstances where a transverse magnetoelectric effect occurs in samples of undoped three-well $Al_xGa_{1-x}As/GaAs$ ($x = 0.25$) heterostructures are presented in Fig. 8. All the data relate to the angle of inclination $\varphi = 45°$ of the heterostructure relative to the direction of the magnetic field, at which, according to formula (13), the effect is at a maximum. It is seen that in all the cases the $P_z(H)$ dependence take the form of symmetrical functions even in H. In the region of weak fields, where the toroid moment grows linearly with increasing field strength, the electric polarization is quadratic in the field, $P_z \sim H^2$. In contrast to the PGE, in which case the U_{PGE} passes through a maximum with an increase in H, the polarization in the transverse MEE continues growing in strong fields with a tendency to saturation, which is a consequence of two factors: a decrease, with increasing field strength, in the toroid moment induced by the lateral component H_z of the field [see formulas (11) and (13)], and a linear growth of the normal component H_x of the field. A comparison of the data on the transverse MEE, measured in heterostructures with tunnel-coupled and separated quantum wells, gives the same picture as that observed in the case of the PGE, namely, in samples with separated quantum wells the effect is considerably less delineated (cf. curves *1* and *1a* in Fig. 8c). The measurements of the transverse MEE, performed at different angles of inclination of the heterostructure plane to the direction of the magnetic field (Fig. 8d), showed that the angular dependence of the polarization follows expression (13) with a good accuracy.

Photogalvanic effect and transverse magnetoelectric effect in the doped heterostructure of the AlGaAs/InGaAs/GaAs system. Figure 9a displays the results of measurements of the field dependences $U_{PGE}(H)$ at room temperature in

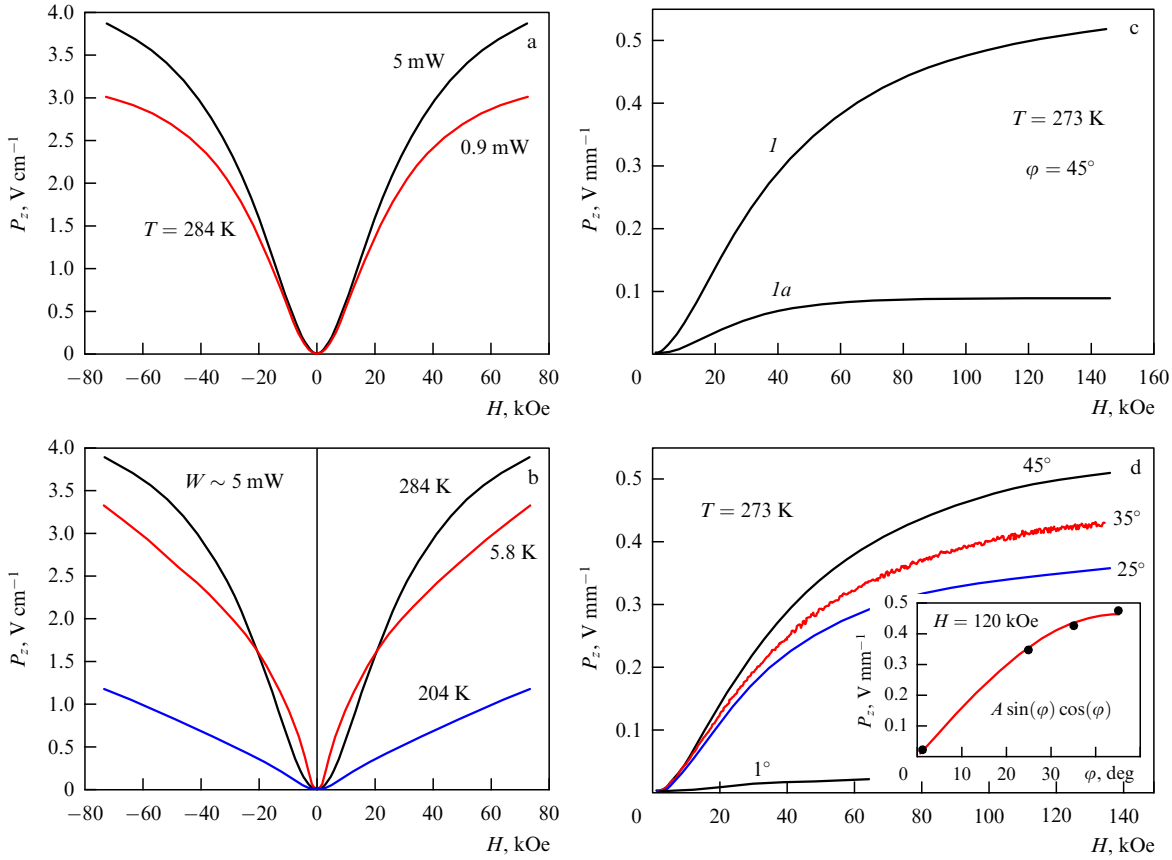

Figure 8. Field dependences of electric polarization $P_z(H)$ in the case of occurrence of the transverse magnetoelectric effect in samples of asymmetric three-well undoped $Al_xGa_{1-x}As/GaAs$ ($x = 0.25$) heterostructures: (a) for the S1 structure at room temperature and illumination powers $W = 5$ and 0.9 mW; (b) for the S1 structure at $W = 5$ mW and $T = 273$, 204, and 4.2 K; (c) for heterostructures with different tunnel coupling (curves *1* and *1a* refer to the structures S1 and S1a, respectively; see Table 1), and (d) at different inclinations of the heterostructure (S1) to the direction of the magnetic field (in the inset to the figure, the angular dependence of P_z at $H = 120$ kOe is given). The values of P_z are given in volts per unit length of the illuminated section of the heterostructure.

magnetic fields of up to 75 kOe in a sample of the doped heterostructure S512; shown in Fig. 9b are the results of measurements of the $P_z(H)$ dependences in the conditions of occurrence of the transverse magnetoelectric effect (the angle of inclination of the heterostructure with respect to the direction of the magnetic field is $\alpha = 45°$) in magnetic fields up to 140 kOe at room temperature (curve *1*) and at the liquid-helium temperature (curve *2*).

The measurements were made on adjacent potential contacts located at a distance of 0.27 mm from each other. The illumination was accomplished with a halogen lamp, which ensured, at a radiation power supplied to the sample on the order of 5 mW, a power density on the surface of the sample equal to 0.35 mW mm^{-2}. It follows from the comparison of the magnitudes of U_{PGE} at the maximum of the $U_{PGE}(H)$ dependence and of the electric polarization P_z in the region of its saturation in strong magnetic fields with the corresponding values for the undoped S1 heterostructure that at room temperature under equal illumination conditions the values of U_{PGE} and P_z reduced to a unit length of the illuminated section of the sample for the doped structure are less by a factor of approximately 3000.

The magnetoelectric effect in the doped structure, in contrast to that in the undoped structure, strongly depends on temperature: as the temperature decreases from room temperature to 4.2 K, P_z in the doped structure decreases by approximately an order of magnitude (see curve *2* in Fig. 9b). In this case, as can be seen from the data given, in the region of strong magnetic fields noticeably pronounced oscillations of $P_z(H)$ are observed. The period of these oscillations in the inverse magnetic field strength coincides with the period of oscillations for the Shubnikov–de Haas effect when measuring the field dependences of magnetoresistance in the case where the magnetic field is directed along the normal to the surface of the sample.

Both these facts, i.e., the strong weakening of the magnetoelectric effect with decreasing temperature and the presence of oscillations in the $P_z(H)$ dependence at low temperatures, indicate the above-mentioned participation of equilibrium carriers in the compensation for the electric polarization that arises due to the nonequilibrium photoinduced fraction of charge carriers. It is understandable that the extent of this compensation must be determined by the relaxation time τ in electron transport and, correspondingly, by the conductivity of the system ($\tau \ll \tau_r$, where τ_r is the recombination time of the photoinduced carriers). As the temperature decreases from room temperature to 4.2 K, the relaxation time τ increases substantially, which leads to an even larger compensation (in comparison with that observed at room temperature) for the electric dipole moment induced by the magnetic field, which, in addition, in strong magnetic fields ($\omega_c\tau \gg 1$, where ω_c is the cyclotron frequency) begins oscillating with the magnetic field.

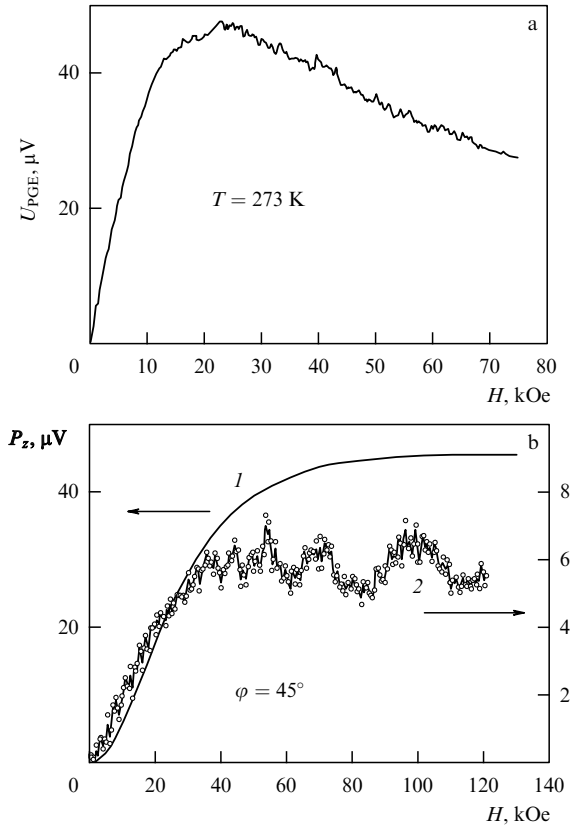

Figure 9. Field dependences of the photogalvanic effect: at $T = 273$ K (a), and electric polarization P_z in the transverse magnetoelectric effect (b) at $T = 273$ K (curve *1*) and 4.2 K (curve *2*) for a sample of an asymmetric doped S512 heterostructure.

3. At present, diverse manifestations of a new type of ordering are being experimentally discovered in condensed systems, namely, of toroidal ordering which was predicted at the beginning of the 1980s. A significant role in this discovery has been played by the methods of engineering the energy-band structure, which made it possible to observe the specific features of anomalous photogalvanic and magnetoelectric effects described in this report under nonequilibrium conditions in artificially grown heterostructures. Of large interest is the study of the possibility of existing a superdiamagnetic state in spatially inhomogeneous toroics, which is connected with the concept of a pseudomagnetic field [16] acting on the charge carriers.

It should be also noted that the magnetic field can break the symmetry of intrasubband transitions and lead to the occurrence of an APGE connected with the appearance of an additive, asymmetric in momentum, to the distribution function, which apparently was observed in work [47]. It is significant that the symmetry of the experiment in this case also allows the existence in the system of a toroid moment and allied asymmetry of the spectrum with respect to the quasimomentum, which can be responsible for the APGE examined in this report. A comparison and the revealing of differences in the experimental manifestations of the two mechanisms of the APGE — caused by the asymmetry of the distribution function in momentum in the symmetric in the electric field approximation [40, 47] and caused by the asymmetry of the spectrum [see Eqns (7)–(9)] — require additional study.

References

1. Gorbatsevich A A, Kapaev V V, Kopaev Yu V *Ferroelectrics* **161** 303 (1994)
2. Gorbatsevich A A, Kopaev Yu V *Ferroelectrics* **161** 321 (1994)
3. Landau L D, Lifshitz E M *Statisticheskaya Fizika* (Statistical Physics) Pt. 1 (Moscow: Nauka, 1976) p. 489 [Translated into English (Oxford: Pergamon Press, 1980)]
4. Ascher E, in *Magnetoelectric Interaction Phenomena in Crystals* (Eds A J Freeman, H Schmid) (New York: Gordon and Breach Sci. Publ., 1975) p. 69
5. Volkov B A, Gorbatsevich A A, Kopaev Yu V *Zh. Eksp. Teor. Fiz.* **86** 1870 (1984) [*Sov. Phys. JETP* **59** 1087 (1984)]
6. Smolenskii G A, Chupis I E *Usp. Fiz. Nauk* **137** 415 (1982) [*Sov. Phys. Usp.* **25** 475 (1982)]
7. Schmid H *Ferroelectrics* **162** 317 (1994)
8. Kimura T et al. *Nature* **426** 55 (2003)
9. Hur N et al. *Nature* **429** 392 (2004)
10. Eerenstein W, Mathur N D, Scott J F *Nature* **442** 759 (2006)
11. Ginzburg V L, Gorbatsevich A A, Kopaev Yu V, Volkov B A *Solid State Commun.* **50** 339 (1984)
12. Zel'dovich Ya B *Zh. Eksp. Teor. Fiz.* **33** 1531 (1957) [*Sov. Phys. JETP* **6** 1184 (1958)]
13. Ascher E *Helv. Phys. Acta* **39** 40 (1966)
14. Ascher E *Int. J. Magn.* **5** 287 (1974)
15. Landau L D (unpublished)
16. Gorbatsevich A A *Zh. Eksp. Teor. Fiz.* **95** 1467 (1989) [*Sov. Phys. JETP* **68** 847 (1989)]
17. Dubovik V M, Cheshkov A A *Fiz. Elem. Chastits At. Yadra* **5** 791 (1974) [*Sov. J. Part. Nucl.* **5** 318 (1974)]
18. Dubovik V M, Tosunyan L A *Fiz. Elem. Chastits At. Yadra* **14** 1193 (1983) [*Sov. J. Part. Nucl.* **14** 504 (1983)]
19. Landau L D, Lifshitz E M *Teoriya Polya* (The Classical Theory of Fields) (Moscow: Nauka, 1988) p. 136 [Translated into English (Oxford: Pergamon Press, 1983)]
20. Spaldin N A, Fiebig M, Mostovoy M *J. Phys. Condens. Matter* **20** 434203 (2008)
21. Dubovik V M, Krotov S S, Tugushev V V *Kristallografiya* **32** 540 (1987) [*Sov. Phys. Crystallogr.* **32** 314 (1987)]
22. Dubovik V M, Tugushev V V *Phys. Rep.* **187** 145 (1990)
23. Sannikov D G *Pis'ma Zh. Eksp. Teor. Fiz.* **41** 229 (1985) [*JETP Lett.* **41** 277 (1985)]
24. Sannikov D G, Zheludev I S *Fiz. Tverd. Tela* **27** 1369 (1985) [*Sov. Phys. Solid State* **27** 826 (1985)]
25. Ederer C, Spaldin N A *Phys. Rev. B* **76** 214404 (2007)
26. Popov Yu F et al. *Pis'ma Zh. Eksp. Teor. Fiz.* **69** 302 (1999) [*JETP Lett.* **69** 330 (1999)]
27. Popov Yu F et al. *Zh. Eksp. Teor. Fiz.* **114** 263 (1998) [*JETP* **87** 146 (1998)]
28. Van Aken B B et al. *Nature* **449** 702 (2007)
29. Affleck I, Marston J B *Phys. Rev. B* **37** 3774 (1988)
30. Shoenberg D *Magnetic Oscillations in Metals* (Cambridge: Cambridge Univ. Press, 1984) [Translated into Russian (Moscow: Mir, 1986)]
31. Privorotskii I A *Zh. Eksp. Teor. Fiz.* **52** 1755 (1967) [*Sov. Phys. JETP* **25** 1167 (1967)]
32. Girvin S M, MacDonald A H *Phys. Rev. Lett.* **58** 1252 (1987)
33. Zhang S C, Hansson T H, Kivelson S *Phys. Rev. Lett.* **62** 82 (1989)
34. Volovik G E *The Universe in a Helium Droplet* (New York: Oxford Univ. Press, 2003)
35. Kalmeyer V, Laughlin R B *Phys. Rev. Lett.* **59** 2095 (1987)
36. Halperin B I, March-Russell J, Wilczek F *Phys. Rev. B* **40** 8726 (1989)
37. Sawada K, Nagaosa N *Phys. Rev. Lett.* **95** 237402 (2005)
38. Jung J H et al. *Phys. Rev. Lett.* **93** 037403 (2004)
39. Belinicher V I, Sturman B I *Usp. Fiz. Nauk* **130** 415 (1980) [*Sov. Phys. Usp.* **23** 199 (1980)]
40. Ivchenko E L, Pikus G E, in *Problemy Sovremennoi Fiziki: Sbornik Statei k 100-letiyu so Dnya Rozhdeniya A.F. Ioffe* (Problems of Modern Physics: Collected Papers on the Occasion of Centenary of the Birth of A.F. Ioffe) (Exec. Ed. A P Aleksandrov) (Leningrad: Nauka, 1980) p. 275

41. Ivchenko E L, Pikus G E *Superlattices and Other Heterostructures: Symmetry and Optical Phenomena* (Springer Series in Solid-State Sciences, Vol. 110) 2nd ed. (Berlin: Springer, 1997)
42. Sturman B I, Fridkin V M *Fotogal'vanicheskii Effekt v Sredakh bez Tsentra Simmetrii i Rodstvennye Yavleniya* (Photogalvanic Effect in Media without a Center of Symmetry and the Related Phenomena) (Moscow: Nauka, 1992)
43. Gorbatsevich A A, Kapaev V V, Kopaev Yu V *Pis'ma Zh. Eksp. Teor. Fiz.* **57** 565 (1993) [*JETP Lett.* **57** 580 (1993)]
44. Omel'yanovskii O E, Tsebro V I, Kadushkin V I *Pis'ma Zh. Eksp. Teor. Fiz.* **63** 197 (1996) [*JETP Lett.* **63** 209 (1996)]
45. Tsebro V I et al. *Phys. Low-Dim. Struct.* (1/2) 25 (1997)
46. Aleshchenko Yu A et al. *Pis'ma Zh. Eksp. Teor. Fiz.* **58** 377 (1993) [*JETP Lett.* **58** 384 (1993)]
47. Emelyanov S A, Meltser B Ya, Ivanov S V *Pis'ma Zh. Eksp. Teor. Fiz.* **76** 547 (2002) [*JETP Lett.* **76** 469 (2002)]

PACS numbers: **75.80.+q**, **77.80.–e**
DOI: 10.3367/UFNe.0179.200908i.0897

Inhomogeneous magnetoelectric interaction in multiferroics and related new physical effects

A K Zvezdin, A P Pyatakov

1. Introduction

In this report, we consider a variety of phenomena related to inhomogeneous magnetoelectric interaction. The interconnection between the spatial modulation of the order parameter and electric polarization, known as the flexoelectric effect in liquid crystals, in the case of multiferroics manifests itself in the form of spin modulation induced by electric polarization, and as an inverse effect of formation of spin-induced electric polarization. This *flexomagnetoelectric* interaction also underlies the influence of the ferroelectric domain structure on the antiferromagnetic structure and the magnetoelectric properties of micromagnetic structures. We also consider the influence of an inhomogeneous magnetoelectric effect on the dynamic properties of multiferroics, in particular, on the magnon spectra.

The last decade has been characterized by a spate of interest in media with interrelated magnetic and electrical properties* (see reviews [1–10], and also special issues of two journals devoted to this problem [11]). The interest in this area is expressed, on the one hand, by enhanced attention paid to the fundamental aspects of magnetoelectric phenomena in multiferroics (substances in which magnetic and electric orderings coexist), and, on the other hand, by the expectation of concrete practical applications of magnetoelectrics in spin electronics (in particular, as the base for magnetic-memory devices) and in sensor technology.

The application of multiferroics will make it possible to significantly enlarge the functional possibilities of spintronics: a new degree of freedom — electric polarization — provides the additional means to tune the magnetic and magnetoresistive properties of spintronic elements [12] and to realize four-state logical units [13, 14]. Moreover, the use of magnetoelectric phenomena will make it possible in perspective to avoid using electric currents for magnetic recording [15–18], which is quite timely, since the progressively developing miniaturization of the traditionally used inductive elements is encountering the problem of excessive heat release because of an increase in the current density [19].

An enhanced interest in the fundamental mechanisms of interaction between magnetic and electric subsystems in solids has also been observed lately [10, 20–27], and the variety of types of magnetoelectric interactions has grown noticeably. In the classical review [28], which reflected the level of knowledge on multiferroics in the early 1980s, it was assumed that the polarization $\mathbf{P}$ and the magnetizations $\mathbf{M}_s$ of the sublattices (here s is the order number of a magnetic sublattice) were coupled mainly via the interaction of the form

$$F^{\mathrm{ME}} = -\frac{1}{2}\sum_{ss'} \gamma_{ss'}^{ijkl} P^i P^j M_s^k M_{s'}^l ,$$

which did not require any additional conditions except for the very existence of magnetic and electric ordering; recently, however, other interaction modes, introduced in Ref. [28], have come to the foreground, namely, those that are linear in the order parameters. In particular, the association of electric polarization with the presence of spatially modulated spin structures in the substance was established [29–31], and effects odd with respect to field, which make it possible to control the magnetic structure with the aid of an electric field, have also been discovered [32–35]. Whatever the origin of spatial modulation, i.e., whether as a result of competing exchange interactions, as in frustrated multiferroics [29–33], as a result of the magnetoelectric nature, as in bismuth ferrite [1, 36], or as a result of establishing equilibrium micromagnetic configuration [34, 35], in all cases nonzero spatial derivatives of the magnetic order parameter, $\nabla_i M_j$, existed, which created prerequisites for the manifestation of inhomogeneous *magnetoelectric interaction*.

2. Inhomogeneous magnetoelectric (flexomagnetoelectric) interaction

The inhomogeneous magnetoelectric interaction of the $P_i n_j \nabla_k n_l$ type, where $\mathbf{n}$ is the unit vector of the magnetic order parameter (magnetization or the antiferromagnetic vector), was introduced in Refs [37, 38] in connection with the possibility of the appearance, in magnetically ordered crystals, of long-period structures, and with the possibility of the manifestation of the inverse effect of the formation of electric polarization at domain boundaries [39]. The close analogy between the spatially modulated spin structures in ferroelectromagnets and the spatial modulation of the director in nematic liquid crystals has been noted in Ref. [40]: it manifests itself in the similarity of the mathematical expressions for the energy of inhomogeneous magnetoelectric interaction in ferroelectromagnets and the energy of flexoelectric interaction in liquid crystals, where the director $\mathbf{n}$ serves as the order parameter. This gives grounds to call the inhomogeneous magnetoelectric interaction the *flexomagnetoelectric* interaction.

In the isotropic case or in the case of cubic symmetry, the inhomogeneous magnetoelectric interaction, to an accuracy of the total derivative, takes on an elegant form [40]

$$F_{\mathrm{flexo}} = \gamma \mathbf{P}\big(\mathbf{n}\,\mathrm{div}\,\mathbf{n} + [\mathbf{n}\times \mathrm{rot}\,\mathbf{n}]\big) . \qquad (1)$$

* Since the mid-1990s, the number of published works devoted to magnetoelectric materials has increased twofold–threefold every five years, and has reached about 800 publications per year.

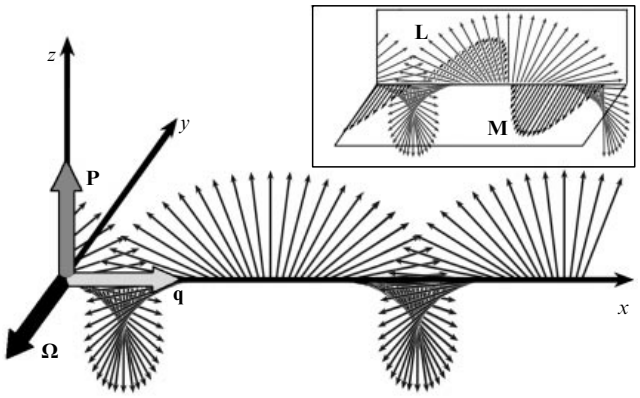

Figure 1. Spin cycloid and three mutually perpendicular vectors: rotation axis **Ω**, direction of modulation **q**, and polar vector **P**. In the inset: spin cycloid $\mathbf{L}(x)$ in the vertical plane is accompanied in bismuth ferrite by a wave of magnetization $\mathbf{M}(x)$ in the horizontal plane xy.

A very visual image, which illustrates the interconnection between the polarization **P**, the wave vector **q** of the spatially modulated structure, and the rotation axis **Ω** of spins, is given in Ref. [23]: these vectors form a trio of mutually perpendicular vectors $\mathbf{P} \sim [\mathbf{\Omega} \times \mathbf{q}]$ (Fig. 1).

It follows from this simple rule that in ferroelectrics we can expect the appearance of cycloidal ($\mathbf{q} \perp \mathbf{\Omega}$) rather than helicoidal ($\mathbf{q} \parallel \mathbf{\Omega}$) type spatially modulated structures, while for the domain boundaries to manifest electrical properties, the magnetization in them must rotate in the plane perpendicular to the domain (the Néel type domain walls).

3. Spatially modulated spin structure in bismuth ferrite $BiFeO_3$

One of first multiferroics in which a spatially modulated spin structure was discovered was bismuth ferrite ($BiFeO_3$) compound [41]. Later on, it was established that the structure has a magnetoelectric origin: bismuth ferrite represents an intrinsic ferroelectric, and the spatial modulation of spins in it is stabilized by spontaneous polarization as a result of flexomagnetoelectric interaction (1) [42, 43].

It is interesting that the detection of a spin cycloid and the establishment of its nature made it possible to explain why one more multiferroic property allowable by the magnetic symmetry — weak ferromagnetism — could not long be revealed in bismuth ferrite. The reason was that because of the presence of a spatially modulated structure in bismuth ferrite, the value of the spontaneous magnetic moment, which is proportional to the x component of the antiferromagnetic vector **L**, periodically reversed its sign and was equal to zero, on average, within the period (see inset to Fig. 1). The observation of a weak ferromagnetic moment became possible only upon the suppression of the spin cycloid and transition to a uniform antiferromagnetic state [44].

The transition between the homogeneous and incommensurate phases can be considered as a spontaneous nucleation of domain boundaries whose energy is written as

$$F_{\mathrm{DW}} = 4\sqrt{AK_u} - \pi\gamma P_{\mathrm{s}}\,, \tag{2}$$

where P_{s} is the spontaneous electric polarization, the constants A and K_u determine the energy of the inhomogeneous exchange and the uniaxial magnetic anisotropy, respectively:

$$F_{\mathrm{exch}} = A\sum_{i=x,y,z}(\nabla n_i)^2 = A\left[(\nabla\theta)^2 + \sin^2\theta\,(\nabla\varphi)^2\right], \tag{3}$$

$$F_{\mathrm{an}} = -K_u\cos^2\theta\,, \tag{4}$$

and the polar angle θ is counted from the z-axis oriented along the c-axis of the crystal (see Fig. 1). The second term in the energy (2) of domain boundaries is obtained by the integration of the flexomagnetoelectric interaction (1) over the period of the structure. Thus, the condition for the phase transition, $F_{\mathrm{DW}} = 0$, takes on the form

$$\gamma = \frac{4}{\pi P_{\mathrm{s}}}\sqrt{AK_u}\,. \tag{5}$$

Formula (5) can also be obtained from the condition of the equality of the thermodynamic energies of the homogeneous and incommensurate phases in which the distribution of the magnetic parameter is described by elliptic functions [43, 45].

In the literature, another method of obtaining the conditions for phase transition also occurs, based on the harmonic approximation [36] in which it is considered that the components of the order parameter **n** change according to the law $n_i(x) \sim \sin(qx + \phi_i)$. This approach, though approximate, makes it possible to arrive at numerical estimates with an almost 10% accuracy [45].

Condition (5) can also be used for evaluating the critical magnetic field H_{c} of the induced phase transition. In this case, the uniaxial anisotropy in formula (5) in an external magnetic field H must be replaced by the effective anisotropy $K_{\mathrm{eff}}(H) = K_u - \chi_\perp H^2/2$, where $\chi_\perp$ is the magnetic susceptibility in the direction perpendicular to the antiferromagnetic vector at $H \parallel c$. In the general case of an arbitrary orientation of the magnetic field, the magnitude of H_{c} will depend on its orientation relative to the plane of the cycloid (see Appendix).

The effective magnetic anisotropy can also change under the effect of other factors, for instance, the presence of impurities of rare-earth ions, magnetostrictive contributions caused by epitaxial stresses that arise upon deposition of a substance onto a substrate with a somewhat different lattice parameter, etc. These reasons were used to explain the suppression of the spin cycloid and the appearance of weak ferromagnetism in strong magnetic fields in bismuth ferrite-based compounds doped with rare-earth ions and in thin films [1, 46]. The latter caused a wave of interest in studying bismuth ferrite and made it the most popular subject (among multiferroics) of both fundamental and applied studies (see the reviews [1, 8, 44, 47, 48]).

4. Antiferromagnetic ordering in bismuth ferrite films with a stripe ferroelectric domain structure

As was shown in numerous studies, no spatially modulated spin structure is observed in thin films (with a thickness of less than 500 nm) of bismuth ferrite [46] (see also reviews [5, 8] and the references cited therein). However, this does not mean that the inhomogeneous magnetoelectric interaction does not manifest itself in any way. Even in the homogeneous antiferromagnetic state a ferroelectric domain structure can be observed [49–51], which, as shown in Ref. [52], can modulate the antiferromagnetic vector by means of flexomagnetoelectric interaction. The inhomogeneous magnetoelectric interaction (1) manifests itself in a jump of the derivative $\nabla\theta$ at the boundary between the ferroelectric

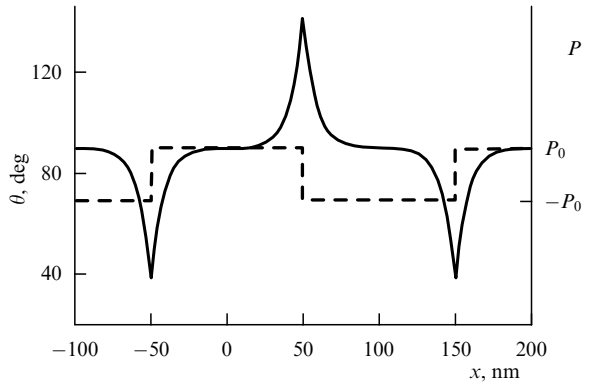

Figure 2. Modulation of the direction of the antiferromagnetic vector (solid curve, left-hand scale) under the effect of a ferroelectric domain structure (dashed curve, right-hand scale) in multiferroics with a flexomagnetoelectric interaction [52].

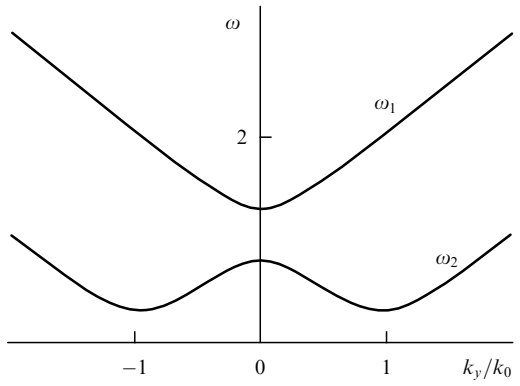

Figure 3. The appearance of a minimum in the dispersion relation for the low-frequency branch of a homogeneous antiferromagnet with a flexomagnetoelectric interaction (k_0 is the magnitude of the cycloid wave vector in the spatially modulated state [61]).

domains with the electric polarizations directed upward (+) and downward (−):

$$A(\nabla\theta)\Big|_{-}^{+} = \gamma P\Big|_{-}^{+} = 2\gamma P_{\rm s}\,. \qquad (6)$$

A graphic representation of the modulation of the direction of the antiferromagnetic vector, assigned by the angle θ, is displayed in Fig. 2.

Thus, in the presence of a ferroelectric domain structure the homogeneous antiferromagnetic state is not the ground one. If in the material there coexist antiferromagnetic and ferroelectric domain structures, then the above effect can manifest itself in the form of the pinning of the antiferromagnetic domain structure to the ferroelectric domain boundaries, which was indeed examined experimentally in manganites [53].

5. Influence of a flexomagnetoelectric interaction on the magnon spectrum in multiferroics

The presence, albeit in a latent form, of a flexomagnetoelectric interaction in the homogeneous antiferromagnetic state shows itself not only in static structures, but also in the dynamic properties of antiferromagnets, namely, in the spectra of magnon excitations which in multiferroics acquire a new quality — the property of *electromagnons* [54]. The influence of a flexomagnetoelectric interaction on the magnon spectra in multiferroics with modulated structures was considered in Refs [55–58].

In films, spatially modulated structures are absent and, therefore, the magnetoelectric interaction (1) does not seem to be urgent for them. It is precisely on this assumption that the problem of the magnon spectrum in bismuth ferrite films was solved in the recent work [59]. However, as was shown in Refs [60, 61], flexomagnetoelectric interaction (1) exerts a substantial effect on the spectrum and properties of magnons in a homogeneous state as well: a minimum appears in their dispersion relation at finite wave vectors for the waves propagating in the direction perpendicular to the electric polarization vector in the case of multiferroics [61] or in the direction perpendicular to the external electric field in the case of centrally symmetric ferromagnets [60]. Thus, the inhomogeneous magnetoelectric interaction in thin bismuth ferrite films causes the mutual interaction of two branches of spin waves propagated along the weak ferromagnetic moment $\mathbf{k} \parallel \mathbf{M}_0$ and leads to the appearance of a minimum in the low-frequency branch at the wave vector equal to the wave vector $\mathbf{k}_0$ of the cycloid in a bulk bismuth ferrite sample (Fig. 3), which reflects the development of instability in the system relative to the transition to the inhomogeneous state with increasing flexomagnetoelectric interaction. Furthermore, the presence in the substance of a homogeneous magnetoelectric interaction of the form $\alpha E_i H_j$, together with a flexomagnetoelectric interaction (1), leads to the nonequivalence (nonreciprocity) of the propagation of spin waves along and against the antiferromagnetic vector [61]. The above features can manifest themselves in light scattering (Raman and Mandelstam–Brillouin) and in neutron scattering, which can be employed for determining the parameters of magnetoelectric interactions.

Of no less interest is the practical aspect of the matter, since the magnons in multiferroics can be not only excited but also controlled by an electric field. Recently, interesting ideas have appeared concerning the creation of subminiature logic units based on magnons. The point is that in the semiconductor technology of logic elements, in the transition to nanosizes the problem arises of very strong electric fields (close to threshold) necessary for their functioning. On the other hand, modern alternative spintronic devices based on the effects of giant magnetoresistance and spin moment transfer require high current densities ($\sim 10^6$ A cm^{-2} and greater). In Refs [62, 63] it was suggested that the problem of nanominiaturization can be solved by utilizing long-lived magnons in magnetic dielectrics.

6. Surface flexomagnetoelectric effect

The specific conditions that are realized in thin films of bismuth ferrite led to the suppression of the spatially modulated spin structures existing in a bulk; however, a possible and even more natural situation is the reverse one, i.e., when the presence of the inversion center in the symmetry group of a bulk crystal forbids the flexomagnetoelectric interaction, while the conditions for the formation of a spin cycloid on the surface are created. The main distinction between the interfaces, as well as dimension-reduced systems, and bulk materials lies in the fact that the electrons and atoms of the surface are subject to the action of physical fields that are asymmetric with respect to the operation of spatial inversion. This creates prerequisites for the appear-

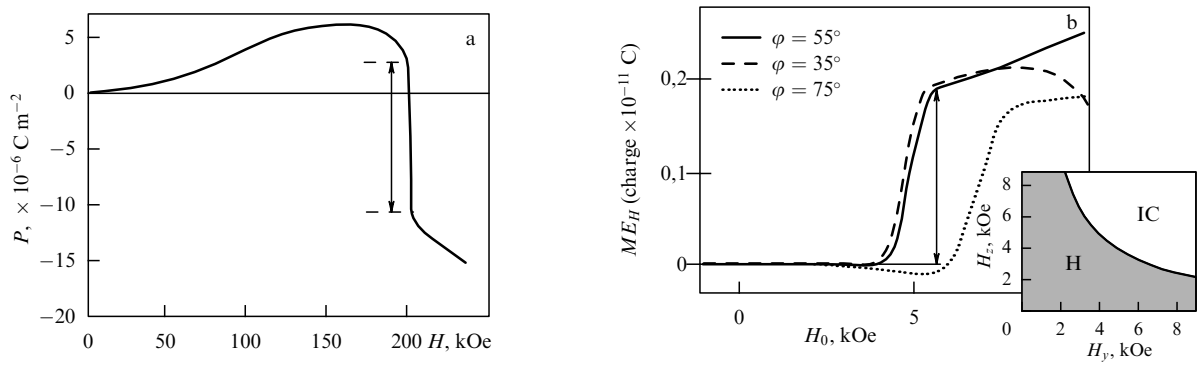

Figure 4. Magnetoelectric anomalies during phase transitions: (a) incommensurate phase–homogeneous state in bismuth ferrite [36], and (b) homogeneous state–incommensurate phase in $BaMnF_4$ [68] (in the inset to the figure, the phase diagram in the $H_y - H_z$ coordinates is given; H, homogeneous antiferromagnetic state, and IC, incommensurate phase).

ance of a flexomagnetoelectric effect in a thin magnetic film or at the interface between magnetic media.

The possibility of the formation of spatially modulated spin structures on the surface and inside thin films of magnetic materials was predicted in Ref. [64], where the condition for the occurrence of a phase transition between the homogeneous and inhomogeneous phases, which is analogous to condition (5), has also been formulated. The same formula is also valid for the boundary between the phases of a liquid crystal, with the difference being that the role of the anisotropy energy with a constant K is played there by the anchoring energy of the liquid-crystal molecules with the substrate, and the role of the exchange stiffness constant A is played by the constant of elastic interaction.

The effect of the formation of spatially modulated spin structures on the surface and inside thin films of magnetic materials was confirmed experimentally in the case of manganese monolayers [65] and in two iron monolayers epitaxially grown on a tungsten substrate with a crystallographic orientation (110) [66]. Using spin-polarized scanning tunneling microscopy, the authors of Ref. [65] observed magnetic modulation with a period of approximately 0.5 nm. The use of probes with a different orientation of the magnetic moment made it possible to establish that this structure in the magnetic monolayer corresponds to a spin cycloid [65], and in the double iron layer to Néel type domain boundaries with a definite chirality [66].

7. Flexomagnetoelectric effect as the origin of improper polarization in multiferroics

As is shown in Section 2, the flexomagnetoelectric interaction (1) in a substance with a broken spatial inversion leads to the formation of modulated spin structures, but the inverse effect is also possible: a spatial spin modulation can result in the elimination of the center of symmetry from the symmetry elements of the crystal and to the appearance of electric polarization.

It is precisely this mechanism that, it is assumed, causes the appearance of electric polarization in orthorhombic manganites $RMnO_3$ (R = Tb [29, 33], Dy [9, 32], Gd [30]), in vanadates $Ni_3V_2O_8$ [67], and in hexaferrites $Ba_2Mg_2Fe_{12}O_{22}$ [31] and explains the magnetoelectric effects observed in these substances, such as the control of the electric polarization by a magnetic field [29, 30] and the inverse effect of the transformation of spatially modulated structures under the action of an electric field [32, 33].

Indeed, as follows from Fig. 1, the reverse of the electric polarization must lead to a change in the relative alignment of the rotation axis and the direction of modulation, i.e., to a change in the chirality of the spiral, which was indeed demonstrated in Refs [32, 33].

In the case of ferroelectrics, such as $BiFeO_3$ and $BaMnF_4$, in which the electric polarization is already present, the spatial spin modulation generates an additional polarization which can be revealed only under special conditions — during phase transitions between the state with spatially modulated spin structures and the homogeneous antiferromagnetic state, i.e., when condition (5) is satisfied.

The flexoelectric polarization emerging at such phase transitions can be determined from the contribution to the thermodynamic potential:

$$\Delta P = -\frac{\partial F_{\text{flexo}}}{\partial E} = \gamma\kappa \frac{\mathrm{d}\theta}{\mathrm{d}x}\,, \tag{7}$$

where κ is the electric susceptibility of the material, $P = \kappa E$, and E is the electric field strength. By averaging over the period of the cycloid, we obtain

$$\langle \Delta P \rangle = \frac{1}{\lambda}\int_0^{2\pi} \Delta P(x) \frac{\mathrm{d}x}{\mathrm{d}\theta}\, \mathrm{d}\theta = \frac{2\pi}{\lambda}\gamma\kappa\,, \tag{8}$$

where λ is the cycloid period.

Figure 4 displays magnetoelectric anomalies manifesting themselves in the form of jumps of the electric polarization in a certain critical field, which can be explained by the phase transitions between the homogeneous and incommensurate phases.

Figure 4a depicts the magnetoelectric dependence for bismuth ferrite. The jump of electric polarization is observed in a critical magnetic field of ~ 200 kOe upon the suppression of the spatially modulated structure. Figure 4b illustrates the different behavior of the magnetoelectric curve for $BaMnF_4$ depending on the angle of inclination of the vector of the magnetic field applied in the plane bc to the b-axis of the crystal, which was observed in the experiments [68], but has not been explained theoretically until now. As we assume, this anomaly reflects the phase transition from the homogeneous antiferromagnetic state to the incommensurate phase upon orientation of the magnetic field at an angle of 45° to the b-axis of the crystal.

Indeed, the $BaMnF_4$ symmetry (class 2, space group $A2_1am$) allows an inhomogeneous magnetoelectric interac-

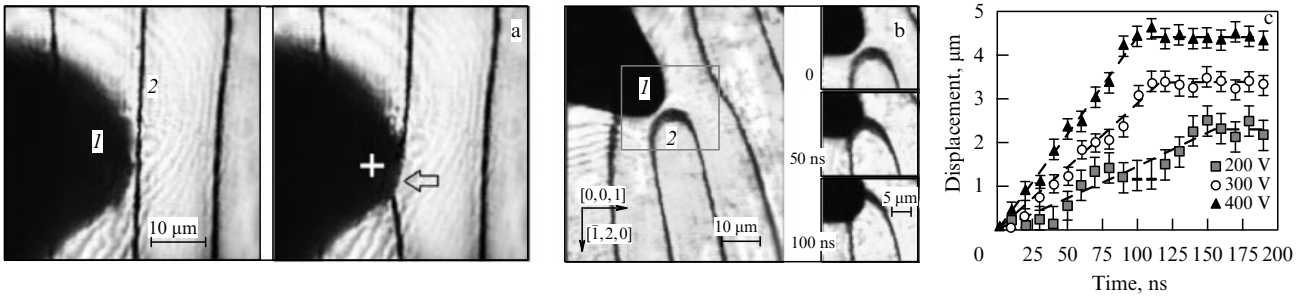

Figure 5. Electric control of the position of a domain boundary in epitaxial iron-garnet films: (a) magneto-optical image of an iron-garnet film in transmitted light (dark lines correspond to boundaries between domains): *1*, electrode; *2*, domain boundary [34]; (b) motion of the head of a magnetic domain caused by an electrostatic action [35], and (c) dependence of the displacement of a domain boundary on time at various potentials at the electrode [35].

tion in the form

$$F_{\text{flexo}} = -(\gamma_{01} + \gamma_{11} H_y H_z)\, P_x \frac{\partial \theta}{\partial x}$$

$$= -\left(\gamma_{01} + \frac{\gamma_{11} H^2}{2} \sin 2\psi\right) P_x \frac{\partial \theta}{\partial x}, \qquad (9)$$

where ψ is the angle made by the magnetic field vector with the *b*-axis of the crystal. This interaction differs from the familiar flexomagnetoelectric interaction (1) in that the coefficient γ in this case can depend on the magnitude and orientation of the external magnetic field. As can be readily seen from expression (9), the magnetoelectric coefficient reaches a maximum value at $\psi = 45^\circ$, and, indeed, the critical magnetic field in this region is a minimum, being approximately 4.5 kOe (Fig. 4b).

It is regrettable that the above-described beautiful effects are observed either at low temperatures, as in $R\text{MnO}_3$ and BaMnF_4, or in high magnetic fields, as in BiFeO_3, which hampers their practical implementation.

8. Iron-garnet films and the flexomagnetoelectric effect at room temperature

Against the background of the wave of enthusiasm caused by the creation of new materials on the base of bismuth ferrite, the prospect for the use of other materials which manifest magnetoelectric properties at room temperature, first and foremost of iron-garnet films, proved to be somewhat underestimated. The linear magnetoelectric effect in these materials, according to estimates made on the basis of measurements of the electroinduced Faraday effect, turned out to be greater by an order of magnitude than that in the classical magnetoelectric material Cr_2O_3 [69].

Furthermore, the iron-garnet films are, perhaps, the most convenient object for an analysis of micromagnetic structures by magneto-optical methods, which acquires special importance in studies of the manifestations of flexomagnetoelectric interactions in micromagnetism. Indeed, the spatial modulation of magnetization can be caused not only by the competition of exchange interactions (as in manganites) or by the inhomogeneous magnetoelectric effect (as in bismuth ferrite), but also by micromagnetic factors such as the minimization of the energy connected with the demagnetizing fields. Since a certain electric polarization can also be associated with such a modulation, the possibility appears of controlling micromagnetic structures with the aid of an electric field.

The influence of an electric field on micromagnetic structures was predicted in many works [23, 39, 40, 70–72]. In this respect, spatially modulated structures such as domain boundaries [39, 70, 72], spin cycloids [40], magnetic vortices [23], and vertical Bloch lines [71] were considered, and it was shown that they are associated with specific distributions of electric polarization. In a recent article, I E Dzyaloshinskii [72] predicted that an electric field that exceeds a certain critical value can induce a magnetic inhomogeneity in the form of a domain wall in a uniformly magnetized medium. This phenomenon, undoubtedly, can be of interest as the prototype of a memory unit with electric recording and a magnetic readout. Unfortunately, no estimates of the threshold field at which the origin of this inhomogeneity occurs were given, but it can be expected that its strength must be significantly high.

If not nucleation, then, at least, the displacement of already existing magnetic domain walls under the action of an electric field was revealed in epitaxial iron-garnet films (about 10 μm thick) grown on the gadolinium-gallium-garnet substrates [34, 35]. Figure 5 demonstrates the effect on the magnetic structure caused by an electric field created by an electrode (pointed copper wire) that touches the dielectric surface of the film [34]. The positive (relative to the substrate) potential at the electrode tip causes an attraction of the domain wall to the electrode (Fig. 5a), while the negative potential leads to its repulsion. After the removal of the voltage, the domain boundary, like a bowed string, returns to the initial equilibrium position. However, the changes caused by the electric field by no means always have a reversible nature: if the system changed from an unstable into a more stable configuration, then the domain boundaries were frozen in the new positions.

The basic features of the effect are as follows:

(1) the effect changed sign upon the change in the electric polarity;

(2) the effect was independent of the polarity of the magnetic domain above which the electrode tip was located (T parity);

(3) the determining role in the effect belongs to the crystallographic orientation of the substrate [the effect was observed in films with the substrate orientation of (210) and (110), and was not observed in (111) films].

All these features indicate the flexomagnetoelectric origin of the effect.

Indeed, both the dependence on the electric polarity and the T parity directly follow from formula (1), and the dependence on the orientation of the substrate is connected

with the distinction between micromagnetic configurations in highly symmetric (111) films and the configurations existing in low-symmetry (110) and (210) films. In (111) films, the direction of the anisotropy axis coincides with the normal to the film, the boundaries between the domains are Bloch type domain walls ($\operatorname{div}\mathbf{M}=0$, $\mathbf{M}\times\operatorname{rot}\mathbf{M}=0$, under the assumption that $|\mathbf{M}|=\text{const}$, which is natural for micromagnetism), and no effect is observed in them, while in the (210) and (110) films the domain boundaries have a Néel component as a result of the inclination of the anisotropy axis with respect to the normal, and the effect becomes different from zero.

The possibility of motion of domain boundaries in an inhomogeneous electric field was noted in Ref. [72]; the velocity of the domain boundary must be proportional to the field gradient. As follows from experimental studies of the dynamics of domain boundaries in pulsed electric fields (Fig. 5b, c), this velocity indeed grows with increasing potential of the electrode tip. The resulting deflection of the domain boundary from the position of equilibrium also grows.

By comparing the results of measurements in an electric field with measurements in a magnetic field, it was possible to determine some quantities that characterize the effect; in particular, the voltage of 500 V (which corresponds to a field strength at the tip equal to 1 MV cm^{-1}) produces the same effect as a magnetic field of 50 Oe [35]. Hence, it is also possible to determine the constant of the effect and from it to estimate the threshold field which, according to Ref. [72], can induce a magnetic inhomogeneity: $E_t = 4\sqrt{KA}/\pi\gamma \sim$ 200 MV cm^{-1}. This magnitude of the threshold field is far from that that can be reached under ambient conditions.

However, the problematic character of the initiation of magnetic structures by an electric field does not yet preclude the prospects of creating devices for magnetic recording on the basis of the flexomagnetoelectric effect, since in the new concept of magnetic memory suggested in Ref. [73] the information recording is achieved by shifting the boundaries between magnetic domains rather than by a reversal of the polarity of a memory element. At the characteristic dimensions of a memory unit of about 100 nm and the velocity of displacement of a domain boundary at a level of 100 m s^{-1} (the order of the velocity given in Ref. [35]), the switching time of the element will be 1 ns.

Acknowledgments

We are grateful to A M Kadomtseva, Yu F Popov, G P Vorob'ev, A A Mukhin, Z V Gareeva, A S Logginov, A V Nikolaev, Hans Schmid, D I Khomskii, and Manuel Bibes for their collaboration and discussions. This work was supported in part by the Russian Foundation for Basic Research, project No. 08-02-01068-a, and Progetto Lagrange-Fondazione CRT.

Appendix

Phase transition induced by a magnetic field

Let us find the dependence of the critical field on its orientation with respect to the plane of the cycloid in a harmonic approximation, assuming that the anisotropy does not affect the shape of the cycloid and that the dependence of the polar angle is described by the linear law

$$\theta = qx\,. \tag{A.1}$$

The wave vector q_0 of the modulated structure, which corresponds to the minimum of the cycloid energy, is found by minimizing contributions to the free energy that depend on the spatial derivatives with respect to the wave vector q [42]. Using Eqns (1) and (2), we obtain

$$\frac{\partial(F_{\text{exch}}+F_L)}{\partial q} = \frac{\partial(Aq^2-\gamma P_z q)}{\partial q} = 0\,. \tag{A.2}$$

For q corresponding to the energy minimum, we have

$$q_0 = \frac{\gamma P_z}{2A}\,. \tag{A.3}$$

In an external field $H=(0,H_y,H_z)$, the contributions to the free energy that correspond to magnetic ordering in a spatially modulated state are written out as

$$F_{\text{cycloid}} = Aq_0^2 - \gamma P_z q_0 - K_u\cos^2\theta - \frac{\chi_\perp H_z^2}{2}\sin^2\theta - \frac{\chi_\perp H_y^2}{2}\,, \tag{A.4}$$

where $\chi_\perp$ is the magnetic susceptibility in the direction perpendicular to the antiferromagnetic vector.

Using (A.3) and averaging the energy over the period λ, we arrive at

$$\langle F_{\text{cycloid}}\rangle_\lambda = -Aq_0^2 - \frac{K_u}{2} - \frac{\chi_\perp H_z^2}{4} - \frac{\chi_\perp H_y^2}{2}\,. \tag{A.5}$$

For a homogeneous state in which the antiferromagnetic vector is perpendicular to the magnetic field and the c-axis ($\theta=90^\circ$, $\varphi=0$), the free energy acquires the form

$$F_{\text{hom}} = -m_s H_x - \frac{\chi_\perp H_z^2}{2} - \frac{\chi_\perp H_y^2}{2}\,, \tag{A.6}$$

where m_s is the magnetization due to weak ferromagnetism.

The critical field of the phase transition, H_c, is found from the condition of the equality of (A.5) with (A.6):

$$H_c = \frac{-2m_s\sin\psi + 2\sqrt{m_s^2\sin^2\psi + \chi_\perp\cos^2\psi\,(Aq_0^2+K_u/2)}}{\chi_\perp\cos^2\psi}\,, \tag{A.7}$$

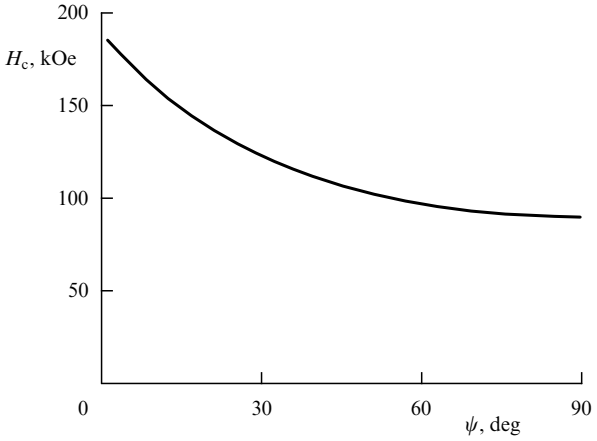

Figure 6. Dependence of the critical field of the phase transition from a spatially modulated state to a homogeneous antiferromagnetic state in bismuth ferrite on the angle of orientation of the field vector with respect to the c-axis.

where ψ assigns the angle of orientation of the field relative to the crystallographic axes: $H_c = (0, H_c \sin\psi, H_c \cos\psi)$.

Figure 6 shows the dependence of the critical field on the angle for the following parameters of the material: $A = 3\times10^{-7}$ erg cm^{-1}, $q_0 = 10^6$ cm^{-1} (corresponding to the cycloid period of 62 nm), $\chi_\perp = 4.7\times10^{-5}$, $m_s \sim 5$ G [45], and $K_u = 3\times10^5$ erg cm^{-3} (including the magnetic anisotropy $K_u^0 = 6\times10^5$ erg cm^{-3} and also the contribution caused by weak ferromagnetism, $K_{DM} = -m_s^2/(2\chi_\perp) \approx -3\times10^5$ erg cm^{-3} [74]). Let us again emphasize that these results were obtained neglecting the deformation of the cycloid shape in an external magnetic field, i.e., on the assumption that the cycloid remains harmonic and is described by dependence (A.1) and by the wave vector q_0 (A.3).

References

1. Zvezdin A K, Pyatakov A P *Usp. Fiz. Nauk* **174** 465 (2004) [*Phys. Usp.* **47** 416 (2004)]
2. Spaldin N A, Fiebig M *Science* **309** 391 (2005)
3. Fiebig M *J. Phys. D* **38** R123 (2005)
4. Turov E A, Nikolaev V V *Usp. Fiz. Nauk* **175** 457 (2005) [*Phys. Usp.* **48** 431 (2005)]
5. Prellier W, Singh M P, Murugavel P *J. Phys. Condens. Matter* **17** R803 (2005)
6. Eerenstein W, Mathur N D, Scott J F *Nature* **442** 759 (2006)
7. Tokura Y *Science* **312** 1481 (2006)
8. Ramesh R, Spaldin N A *Nature Mater.* **6** 21 (2007)
9. Cheong S-W, Mostovoy M *Nature Mater.* **6** 13 (2007)
10. van den Brink J, Khomskii D I *J. Phys. Condens. Matter* **20** 434217 (2008)
11. Kleemann W, Kreisel J (Guest Eds) "Special issue: Current progress in multiferroics and magnetoelectrics" *Phase Transit.* **79** (12) (2006); "Special sections containing papers on multiferroics and manganite" *J. Phys. Condens. Matter* **20** (43) (2008)
12. Gajek M et al. *Nature Mater.* **6** 296 (2007)
13. Béa H et al. *J. Phys. Condens. Matter* **20** 434221 (2008)
14. Scott J F *Nature Mater.* **6** 256 (2007)
15. Binek Ch, Doudin B *J. Phys. Condens. Matter* **17** L39 (2005)
16. Logginov A S, Pyatakov A P, Zvezdin A K *Proc. SPIE* **5955** 56 (2005)
17. Zvezdin A K, Logginov A S, Meshkov G A, Pyatakov A P *Izv. Ross. Akad. Nauk Ser. Fiz.* **71** 1604 (2007) [*Bull. Russ. Acad. Sci. Phys.* **71** 1561 (2007)]
18. Bibes M, Barthélémy A *Nature Mater.* **7** 425 (2008)
19. Chappert C, Fert A, van Dau F N *Nature Mater.* **6** 813 (2007)
20. Spaldin N A, in *Magnetoelectric Interaction Phenomena in Crystals* (NATO Sci. Ser., Ser. II, Mathematics, Physics and Chemistry, Vol. 164, Eds M Fiebig, V V Eremenko, I E Chupis) (Dordrecht: Kluwer Acad. Publ., 2004) p. 87
21. Katsura H, Nagaosa N, Balatsky A V *Phys. Rev. Lett.* **95** 057205 (2005)
22. Sergienko I A, Dagotto E *Phys. Rev. B* **73** 094434 (2006)
23. Mostovoy M *Phys. Rev. Lett.* **96** 067601 (2006)
24. Kimura T, JPSJ Online — News and Comments [November 10, 2006]; http://jpsj.jpap.jp/news/jpsj-nc_20.html
25. Moskvin A S, Drechsler S-L *Phys. Rev. B* **78** 024102 (2008)
26. Nagaosa N *J. Phys. Condens. Matter* **20** 434207 (2008)
27. Lee S et al. *Nature* **451** 805 (2008)
28. Smolenskii G A, Chupis I E *Usp. Fiz. Nauk* **137** 415 (1982) [*Sov. Phys. Usp.* **25** 475 (1982)]
29. Kimura T et al. *Nature* **426** 55 (2003)
30. Kadomtseva A M et al. *Pis'ma Zh. Eksp. Teor. Fiz.* **81** 22 (2005) [*JETP Lett.* **81** 19 (2005)]
31. Ishiwata Sh et al. *Science* **319** 1643 (2008)
32. Milov E V et al. *Pis'ma Zh. Eksp. Teor. Fiz.* **85** 610 (2007) [*JETP Lett.* **85** 503 (2007)]
33. Yamasaki Y et al. *Phys. Rev. Lett.* **98** 147204 (2007)
34. Logginov A S, Meshkov G A, Nikolaev A V, Pyatakov A P *Pis'ma Zh. Eksp. Teor. Fiz.* **86** 124 (2007) [*JETP Lett.* **86** 115 (2007)]
35. Logginov A S et al. *Appl. Phys. Lett.* **93** 182510 (2008)
36. Popov Yu F et al. *Pis'ma Zh. Eksp. Teor. Fiz.* **57** 65 (1993) [*JETP Lett.* **57** 69 (1993)]
37. Vitebskii I M *Zh. Eksp. Teor. Fiz.* **82** 357 (1982) [*Sov. Phys. JETP* **55** 390 (1982)]
38. Bar'yakhtar V G, Yablonskii D A *Fiz. Tverd. Tela* **24** 2522 (1982) [*Sov. Phys. Solid State* **24** 1435 (1982)]
39. Bar'yakhtar V G, L'vov V A, Yablonskii D A *Pis'ma Zh. Eksp. Teor. Fiz.* **37** 565 (1983) [*JETP Lett.* **37** 673 (1983)]
40. Sparavigna A, Strigazzi A, Zvezdin A *Phys. Rev. B* **50** 2953 (1994)
41. Sosnowska I, Neumaier T P, Steichele E *J. Phys. C* **15** 4835 (1982)
42. Sosnowska I, Zvezdin A K *J. Magn. Magn. Mater.* **140–144** 167 (1995)
43. Zalesskii A V et al. *Pis'ma Zh. Eksp. Teor. Fiz.* **71** 682 (2000) [*JETP Lett.* **71** 465 (2000)]
44. Kadomtseva A M et al. *Pis'ma Zh. Eksp. Teor. Fiz.* **79** 705 (2004) [*JETP Lett.* **79** 571 (2004)]
45. Zhdanov A G et al. *Fiz. Tverd. Tela* **48** 83 (2006) [*Phys. Solid State* **48** 88 (2006)]
46. Bai F et al. *Appl. Phys. Lett.* **86** 032511 (2005)
47. Zavaliche F et al. *Phase Transit.* **79** 991 (2006)
48. Haumont R, Kreisel J, Bouvier P *Phase Transit.* **79** 1043 (2006)
49. Chu Y-H et al. *Adv. Mater.* **18** 2307 (2006)
50. Chu Y H et al. *Appl. Phys. Lett.* **90** 252906 (2007)
51. Catalan G et al. *Phys. Rev. Lett.* **100** 027602 (2008)
52. Gareeva Z V, Zvezdin A K *Phys. Status Solidi RRL* **3** 79 (2009)
53. Fiebig M et al. *Nature* **419** 818 (2002)
54. Pimenov A et al. *Nature Phys.* **2** 97 (2006)
55. Popov A I, Esina G A, Zvezdin A K *Fiz. Tverd. Tela* **38** 3091 (1996) [*Phys. Solid State* **38** 1691 (1996)]
56. Katsura H, Balatsky A V, Nagaosa N *Phys. Rev. Lett.* **98** 027203 (2007)
57. Cano A, Kats E I *Phys. Rev.* **78** 012104 (2008)
58. de Sousa R, Moore J E *Phys. Rev. B* **77** 012406 (2008)
59. de Sousa R, Moore J E *Appl. Phys. Lett.* **92** 022514 (2008)
60. Mills D L, Dzyaloshinskii I E *Phys. Rev. B* **78** 184422 (2008)
61. Zvezdin A K, Mukhin A A *Pis'ma Zh. Eksp. Teor. Fiz.* **89** 385 (2009) [*JETP Lett.* **89** 328 (2009)]
62. Kostylev M P et al. *Appl. Phys. Lett.* **87** 153501 (2005)
63. Khitun A, Bao M, Wang K L *IEEE Trans. Magn.* **44** 2141 (2008)
64. Zvezdin A K *Kratk. Soobshch. Fiz. FIAN* (4) 7 (2002)
65. Bode M et al. *Nature* **447** 190 (2007)
66. Heide M, Bihlmayer G, Blügel S *Phys. Rev. B* **78** 140403(R) (2008)
67. Lawes G et al. *Phys. Rev. Lett.* **93** 247201 (2004)
68. Sciau Ph et al. *Ferroelectrics* **105** 201 (1990)
69. Krichevtsov B B, Pavlov V V, Pisarev R V *Pis'ma Zh. Eksp. Teor. Fiz.* **49** 466 (1989) [*JETP Lett.* **49** 535 (1989)]
70. Khalfina A A, Shamsutdinov M A *Ferroelectrics* **279** 19 (2002)
71. Logginov A S et al. *J. Magn. Magn. Mater.* **310** 2569 (2007)
72. Dzyaloshinskii I *Europhys. Lett.* **83** 67001 (2008)
73. Parkin S S P, US Patent 7,031,178 (2006)
74. Ruette B et al. *Phys. Rev. B* **69** 064114 (2004)

PACS numbers: **75.80.+q**, **77.80.–e**
DOI: 10.3367/UFNe.0179.200908j.0904

Terahertz spectroscopy and the magnetoelectric properties of manganite-based multiferroics

A A Mukhin, V Yu Ivanov, V D Travkin, A S Prokhorov, A A Volkov, A V Pimenov, A M Shuvaev, A Loidl

In this report, we present the results of magnetic, magnetoelectric, and terahertz (3–40 cm^{-1}) spectroscopic studies of several manganese multiferroics ($TbMnO_3$, $Eu_{1-x}Y_xMnO_3$, $0 < x \leqslant 0.5$) possessing a spatially modulated spin structure

(sinusoidal, cycloidal) in which, together with the usual magnetically active spin excitations, new modes, namely, electromagnons excited by an electric field, have been discovered. The behavior of these excitations in diverse spontaneous and magnetic-field-induced phase transitions and their connection with the magnetic structure have been studied. It has been established that if the modulated structure is suppressed by a magnetic field, the electromagnons disappear, and this is accompanied by significant changes in the dielectric constant of the multiferroic.

Recently, ever increasing interest has been observed in substances in which magnetic and ferroelectric orderings (multiferroics) coexist and in which the corresponding magnetic and electric degrees of freedom are coupled [1–5]. This not only governs new physical properties of such substances, but also gives the possibility of controlling their state by external magnetic or electric fields, which opens up good prospects for creating new functional materials and devices based on them.

A great response in recent years was generated by the discovery of new classes of multiferroics, in which the ferroelectric ordering has an improper nature and is connected with the specific features of the magnetic structure of these substances, while the magnetoelectric coupling is manifested substantially more strongly than in known ferroelectromagnets [6]. A common feature of such multiferroics is the presence in them of competition (frustration) of exchange interactions and the formation of incommensurate magnetic structures, including those of a cycloidal type, which possess ferroelectric properties.

Such properties were first discovered in some orthorhombic (space group of symmetry *Pbnm*) $R\mathrm{MnO_3}$ (R = Tb, Dy, Gd) manganites [7–10]. In these manganites, at temperatures below the Néel point T_N there is formed a spatially modulated sinusoidal magnetic structure with spins directed along the *b*-axis, which with a further decrease in temperature transforms either to the usual canted antiferromagnetic structure A_yF_z (Eu, Gd) or to a cycloidal (spiral) structure (Tb, Dy) [11], which possesses a spontaneous electric polarization. The reorientation of the electric polarization in a magnetic field, revealed in $\mathrm{TbMnO_3}$ and $\mathrm{DyMnO_3}$ compounds [7–9], testifies to the presence of strong magnetoelectric coupling in these multiferroics.

The presence of this strong magnetoelectric coupling must be manifested in both the static and the dynamic (spectroscopic) properties of these multiferroics and can lead to the appearance of new magnetoelectric excitations. Such spin modes excited by an electric high-frequency field, which are called electromagnons, have been revealed in $\mathrm{TbMnO_3}$ and $\mathrm{GdMnO_3}$ in a terahertz wavelength range in our recent work [12]. A characteristic property of these excitations is that they make a significant contribution to the dielectric constant of the system. Similar electroactive spin excitations were discovered later in the multiferroics $\mathrm{YMn_2O_5}$ and $\mathrm{TbMn_2O_5}$ [13], and $\mathrm{Eu_{1-x}Y_xMnO_3}$ [14–16]. Now, extensive experimental studies are being conducted in this area [17–22]. To explain the observed ferroelectric properties and magnetoelectric spin excitations in multiferroics with modulated spin structures, both phenomenological approaches [23, 24] and microscopic models [25–28] have been proposed; however, no complete explanation of these phenomena exists as yet.

In this report, we present the results of magnetic, magnetoelectric, and terahertz spectroscopic studies of several manganese multiferroics ($\mathrm{TbMnO_3}$, $\mathrm{Eu_{1-x}Y_xMnO_3}$, $0 < x \leqslant 0.5$), part of which have been published in our previous works [12, 15, 16, 20, 29–31]. The transmission spectra $T(\nu)$ were measured using the technique of quasi-optical polarization BWO spectroscopy [32, 33] (BWO is a backward-wave oscillator) in the range of frequencies $\nu = 3-40$ cm^{-1} at temperatures of 3–300 K and magnetic fields of up to 8 T. As specimens, plane-parallel oriented plates of single crystals of manganites with a thickness of about 1 mm and lateral dimensions of approximately 7–9 mm were utilized, which were grown by zone melting with radiation heating. The procedure used makes it possible to obtain spectra of the dielectric (magnetic) constant and the complete set of the parameters of resonance modes, including not only frequencies and widths of lines, but also their intensities (contributions to the dielectric or magnetic susceptibilities) [34].

Let us examine, first, the spectroscopic properties of the most studied manganite $\mathrm{TbMnO_3}$, in which at the Néel point $T_\mathrm{N} \sim 42$ K there appears initially a longitudinal sinusoidal spin-density wave with a wave vector **k** and the direction of spins of $\mathrm{Mn^{3+}}$ along the *crystallographic b-axis*, which, as the temperature decreases to $T \approx 27-28$ K, passes into a cycloidal structure with a vector **k** also directed along the *b*-axis; this transition is accompanied by the appearance of polarization, and for $T < 9$ K an antiferromagnetic ordering of the Tb subsystem occurs [7, 11].

Figure 1 depicts examples of the $\mathrm{TbMnO_3}$ transmission spectra taken using different geometries of experiment. A characteristic property of these transmission spectra is the presence of transmission oscillations due to the interference of the electromagnetic wave in the sample, against the background of which the resonance modes are observed. The most intense absorption lines are observed upon the $\mathbf{e} \parallel a$ polarization (Fig. 1c); they are virtually independent of the polarization of the high-frequency magnetic field **h** and represent electroactive modes (electromagnons) [12]. Notice the presence of a fine structure (splitting) of the electromagnon mode marked by arrows in Fig. 1. In two other polarizations, namely, $\mathbf{h} \parallel c$, $\mathbf{e} \parallel b$ and $\mathbf{h} \parallel b$, $\mathbf{e} \parallel c$, presented in Figs 1a and 1b, respectively, absorption lines are also observed at approximately the same frequencies as for the electromagnons, but their intensity is several orders of magnitude less than the intensity of the electromagnon lines. These weaker lines are identified as the modes characteristic of antiferromagnetic resonance (AFMR).

Figure 2 depicts the temperature dependences of resonance frequencies of modes observed in $\mathrm{TbMnO_3}$. Notice the coincidence of the frequencies of two AFMR modes at the polarizations $\mathbf{h} \parallel c$ and $\mathbf{h} \parallel b$ (designated by empty circles and squares) with the frequencies of the electromagnons excited in the polarization $\mathbf{e} \parallel a$ (shown by solid symbols), which makes it possible to suggest a mixed, magnetoactive and electroactive, nature of these excitations. An analysis reveals that the spin oscillations in this mode correspond to a deflection of the plane of the spin rotation (antiferromagnetic vector) in the cycloid from the crystal plane *bc*, which is accompanied by the appearance of a dynamic component of the electric polarization directed along the *a*-axis. Another AFMR mode (designated in Fig. 2 by triangles), which is excited only by a magnetic field $\mathbf{h} \parallel a$, corresponds to the oscillations of the antiferromagnetic moment in the plane *bc* of the cycloid and is a phason type mode. The lowest-frequency mode at $\mathbf{h} \parallel a$ (inverted triangles), which appears with the ordering of $\mathrm{Tb^{3+}}$ ions, is apparently connected with excitations in the rare-

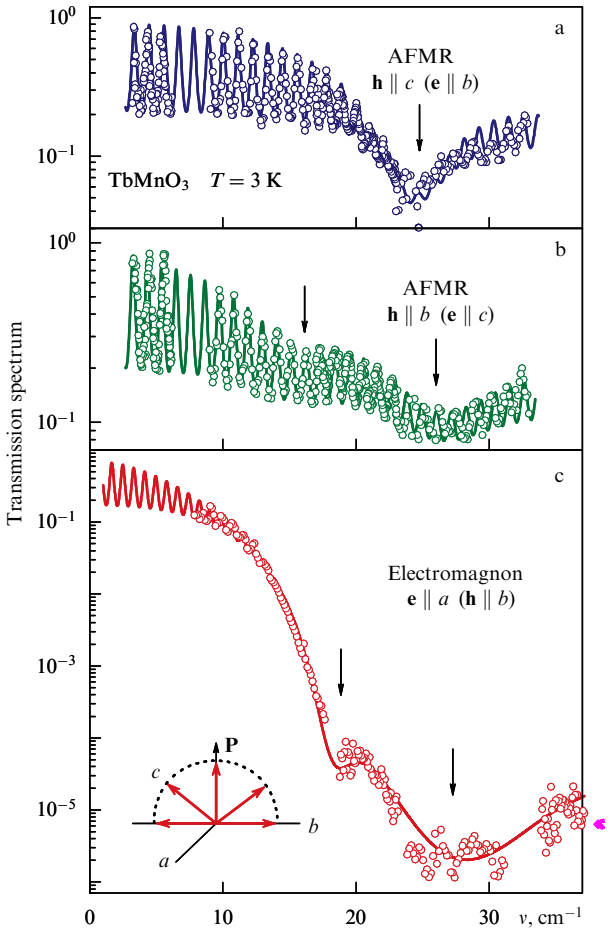

Figure 1. Transmission spectra of plane-parallel plates (~ 1 mm thick) of $TbMnO_3$ [(a, b)—*a* cut, and (c)—*c* cut] at various polarizations of electromagnetic radiation. The inset displays the cycloidal spin structure of Mn^{3+} ions and the polarization vector. Circles correspond to experimental data, while the curves to calculated results.

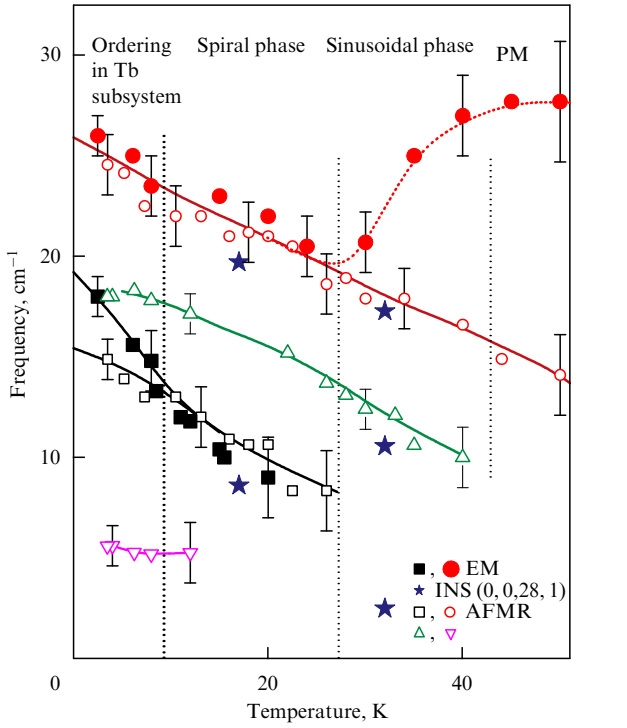

Figure 2. Temperature dependences of the resonance frequencies of various spin excitations in $TbMnO_3$. Solid circles and squares correspond to electromagnons which are observed only at $\mathbf{e} \| a$, and empty symbols correspond to magnetoactive modes of AFMR (Mn subsystem) and excitations of the Tb subsystem (circles—$\mathbf{h} \| b$ and $\mathbf{h} \| c$; squares—$\mathbf{h} \| b$, and triangles—$\mathbf{h} \| a$). In the sinusoidal phase for $T > 27$ K, the frequency positions of the electromagnons are determined only poorly because of a strong broadening; an increase in their frequency reflects in fact the strong increase in their linewidth upon transition to the paramagnetic phase. Asterisks correspond to data on inelastic neutron scattering (INS) [18, 19]. The lines are drawn through the data points only as a guide for eye. The vertical dotted lines separate different phases.

earth subsystem. In the cycloidal ferroelectric phase, the frequencies of the electromagnons and AFMR are sufficiently well identified, in spite of their noticeable widths, but upon transition to the sinusoidal phase for $T > 27$ K the frequency position of the electromagnons is now no longer very definite because of the strong broadening; therefore, the increase in their frequency (see Fig. 2) reflects in fact a strong increase in the linewidth. Note also that at the transition to the paramagnetic phase a noticeable absorption is observed, which appears to be connected with spin fluctuations; in Fig. 2 this is reflected in some curves going into the temperature range that exceeds T_N.

Also shown in Fig. 2 (asterisks) are the frequencies of some modes observed in $TbMnO_3$ with the aid of the inelastic neutron scattering (INS) method [18, 19], which on the whole agree with the excitations discovered by us. Worthy of note is the fact that these modes correspond to inhomogeneous oscillations with the wave vector $k_0 \approx 0.28$ directed along the *b*-axis, which coincides with the wave vector $\mathbf{k}_m$ of the static modulated magnetic structure, $k_m \approx k_0$. Therefore, the excitation of these oscillations in the quasioptical spectra by a practically uniform electromagnetic field with a wave vector $k_{ph} \approx 0$ is accomplished with the participation of Umklapp processes and does not violate the law of conservation of momentum: $k_{ph} = k_m - k_0 \approx 0$.

Examples of the manifestation of electromagnons in the spectra of the real and imaginary parts of the dielectric constant $\varepsilon(\nu) = \varepsilon_1(\nu) + i\varepsilon_2(\nu)$ and their suppression in a magnetic field $\mathbf{B} \| c$ are illustrated in Fig. 3. It is seen that two electromagnon modes observed at $B = 0$ at frequencies of ~ 16 and 24 cm^{-1} disappear upon application of a magnetic field of 8 T along the *c*-axis; under its action, the cycloidal spin structure passes into a usual canted antiferromagnetic phase [8, 9, 12]. In the magnetic field directed along *a*- or *b*-axis, which induces the reorientation of the spin cycloid into the plane *ab*, and of the spontaneous polarization from *c*-axis to *a*-axis, the electromagnon modes are retained and become split into several components [31]. This is indicative of a close interconnection between the electromagnons and the spin structure of the system.

Let us now examine the magnetoelectric and terahertz spectroscopic properties of the new family of multiferroics on the base of yttrium-doped $Eu_{1-x}Y_xMnO_3$ manganites ($0 < x \leqslant 0.5$) [15, 16, 29, 30]. An attractive feature of this system is that it presents the possibility of purposefully controlling and changing the type of magnetic ordering—from the canted antiferromagnetic phase to the spatially modulated magnetic structures that possess a spontaneous electric polarization—by varying the degree of orthorhombic distortions of the crystal lattice and Mn–O–Mn bond angles determining the relationships between the different

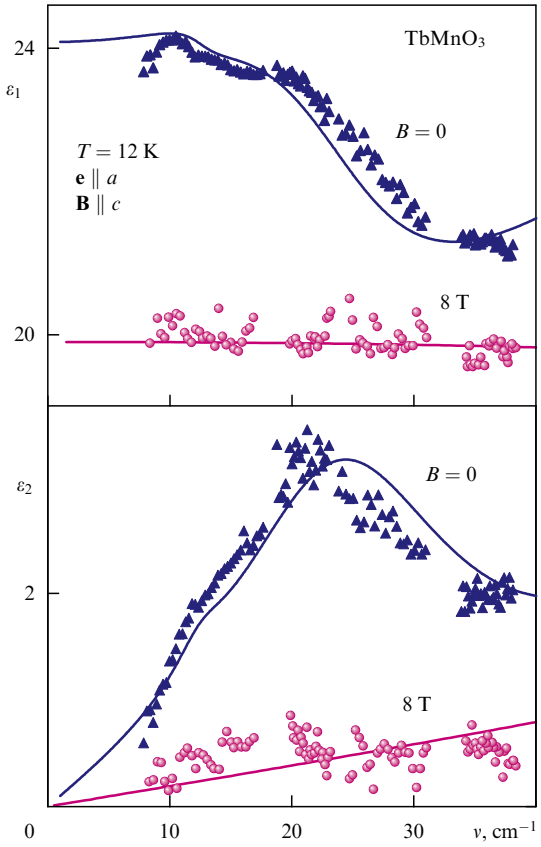

Figure 3. Suppression of electromagnons in a magnetic field $\mathbf{B} \| c$ in the spectra of the real and imaginary parts of the dielectric constant $\varepsilon(\nu) = \varepsilon_1(\nu) + i\varepsilon_2(\nu)$ along the a-axis. In a field of 8 T, the cycloidal spin structure passes into the usual canted antiferromagnetic phase in which the electromagnon disappears.

contributions to the exchange interactions. Furthermore, rare-earth magnetism is virtually absent in this system, which makes it possible to directly follow the Mn subsystem. Studies of magnetic, dielectric, and ferroelectric properties of these systems have revealed the existence of diverse spontaneous and field-induced phase transitions, which indicate the occurrence of a close interconnection between the electric polarization and the magnetic structure [29, 30].

Figure 4a illustrates the examples of temperature dependences of magnetization σ in the magnetic field of 10 kOe, dielectric constants ε, and polarizations P of the crystal $Eu_{0.6}Y_{0.4}MnO_3$. It is seen that the transition to the sinusoidal incommensurate (IC) phase causes a bend in the $\sigma_b(T)$ dependence at T_N, and the subsequent transition to the ferroelectric (FE) cycloidal phase at T_{FE} is accompanied not only by the appearance of polarization P, but also by anomalies in $\sigma_a(T)$, $\varepsilon_a(T)$, and $\varepsilon_c(T)$. Near T_{FE}, a spontaneous reorientation of polarization was revealed from the c-axis to a-axis. At small concentrations ($x < 0.2$), the ground state at low temperatures is already the usual canted antiferromagnetic (CAF) structure into which the system passes from the sinusoidal paraelectric phase. In the intermediate region ($x \sim 0.2$), the behavior of the system has a clearly pronounced hysteretic nature and depends on the sample prehistory: when cooling in the absence of a field, an FE phase is realized up to quite low temperatures, while upon cooling in a rather weak field $\mathbf{H} \| c$ (~ 1 kOe) a transition to a canted antiferromagnetic phase occurs. Figure 4b displays the

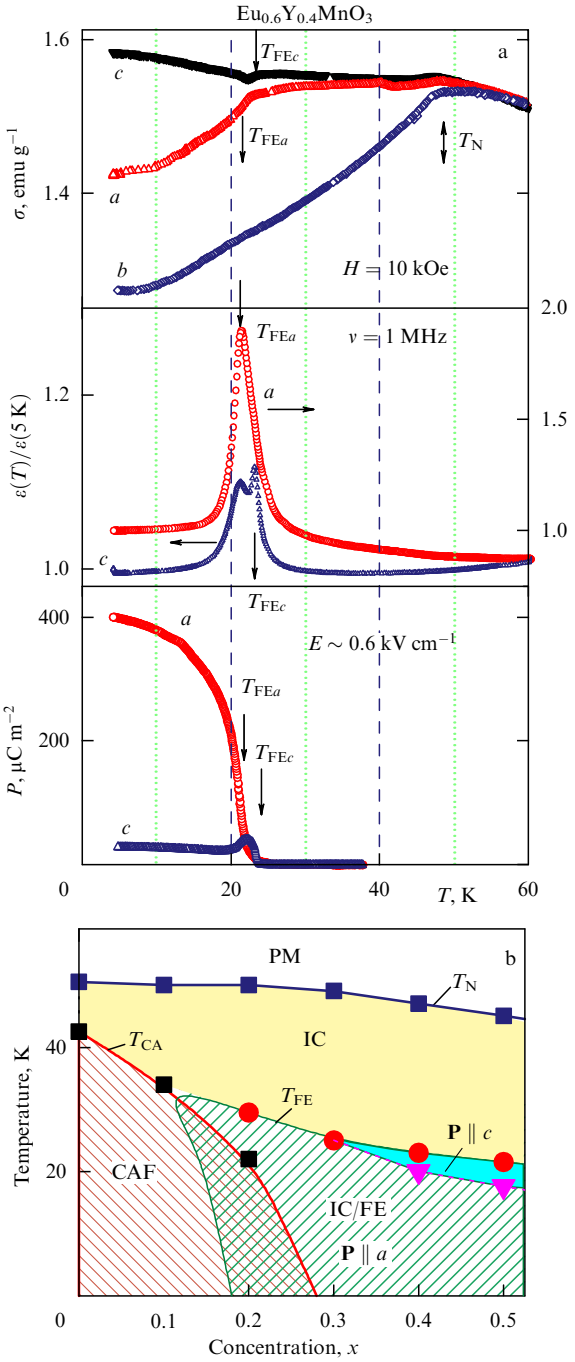

Figure 4. (a) Temperature dependences of the magnetization σ (in a field of 10 kOe), dielectric constant ε (at a frequency $\nu = 1$ MHz), and electric polarization P of an $Eu_{0.6}Y_{0.4}MnO_3$ crystal. The symbols a, b, and c alongside the curves correspond to the crystallographic axis along which the corresponding quantities were measured. In pyroelectric measurements of the polarization, the crystal was preliminarily cooled in an electric field $E \approx 0.6$ kV cm^{-1}. The vertical arrows point to phase transitions. (b) A $T-x$ phase diagram of the $Eu_{1-x}Y_xMnO_3$ system: PM stands for the paramagnetic phase; IC, sinusoidal incommensurate phase; IC/FE, spiral ferroelectric (cycloidal) phase, and CAF, canted antiferromagnetic phase.

$T-x$ phase diagram which illustrates the magnetic and electric states discovered in the $Eu_{1-x}Y_xMnO_3$ system.

Let us now turn to the terahertz spectroscopic properties of $Eu_{1-x}Y_xMnO_3$ compound (see also Refs [15, 16]). Figure 5a displays transmission spectra for a weakly doped $Eu_{0.9}Y_{0.1}MnO_3$ in the polarization $\mathbf{e} \| a$, $\mathbf{h} \| c$, in which,

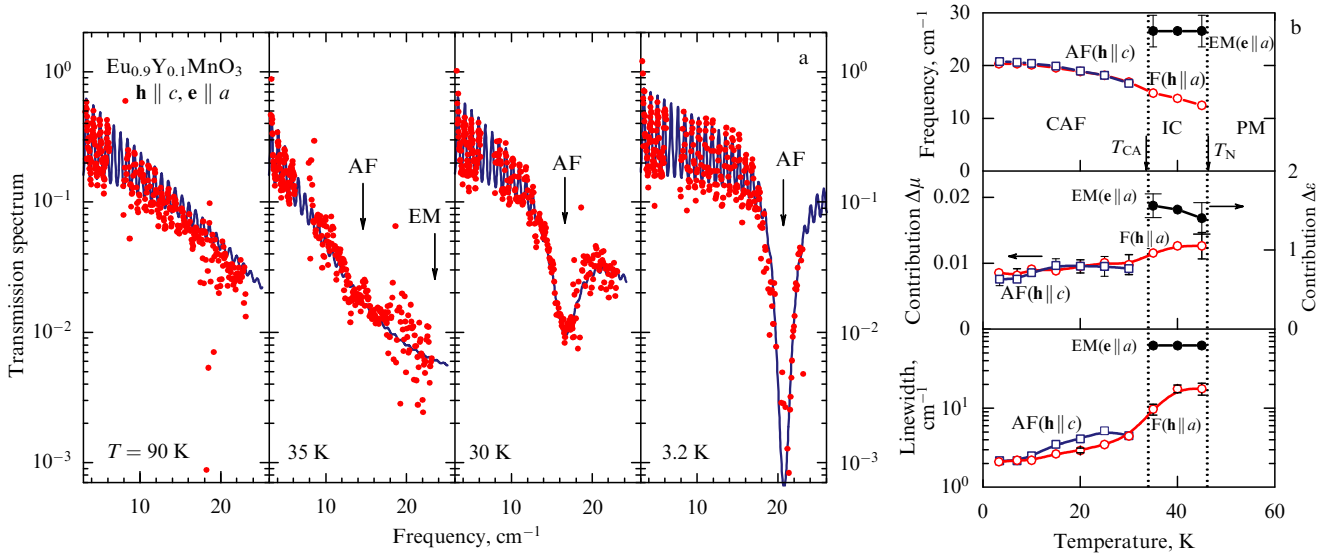

Figure 5. (a) Temperature evolution of the transmission spectra of $Eu_{0.9}Y_{0.1}MnO_3$ in the polarization $\mathbf{e} \parallel a$, $\mathbf{h} \parallel c$ in the course of phase transitions from the paramagnetic (PM) state to a sinusoidal incommensurate (IC) phase and then to a canted antiferromagnetic (CAF) state: points correspond to experimental results, and curves to theoretical calculations. (b) Temperature dependences of resonance frequencies, linewidths, and corresponding contributions to the permittivity or permeability from the electromagnon (EM) and quasiferromagnetic (F) and quasiantiferromagnetic (AF) modes of the AFMR. Vertical dotted lines denote phase boundaries.

according to the phase diagram, a phase transition first occurs to the IC phase and then to the usual CAF state. It is seen that, as the temperature decreases, a wide absorption band appears in the sinusoidal phase (at $T \approx 35$ K), which represents an electromagnon (EM) mode excited by a high-frequency field $\mathbf{e} \parallel a$. Upon phase transition to the canted antiferromagnetic phase, the electromagnon disappears, the sample becomes more transparent, and a relatively narrow absorption line appears (at $T \approx 30$ K), which represents a quasiantiferromagnetic AFMR mode excited by the magnetic field $\mathbf{h} \parallel c$. With a further decrease in temperature, the frequency of this mode grows and the width diminishes.

Figure 5b depicts the temperature dependences of the parameters of the electromagnon and quasiferromagnetic (F) and quasiantiferromagnetic (AF) modes of AFMR, which were obtained by processing transmission spectra with the use of the oscillator model for the frequency dispersion of the permittivity (ε) and permeability (μ). Note the relaxation nature of the electromagnon mode whose linewidth exceeds the frequency, and also the noticeable contribution of this mode, $\Delta\varepsilon \sim 1.5$, to the permittivity. Worthy of note is also a considerable decrease in the linewidths of the F and AF modes of the AFMR upon transition to the canted antiferromagnetic state.

At higher yttrium concentrations, when a cycloidal ferroelectric phase with a polarization along the a-axis becomes the ground state of the system at low temperatures, the electromagnons, as in $TbMnO_3$, represent well identified intense resonance modes observed at $\mathbf{e} \parallel a$. Figure 6 gives, as an example, the low-temperature spectra of the real and imaginary parts of the dielectric constant of an $Eu_{1-x}Y_xMnO_3$ compound at $x = 0.2$ and 0.5, which clearly demonstrate these modes. They have close frequencies, and their contribution to the dielectric constant grows substantially with an increase in the concentration x (from $\Delta\varepsilon \sim 2$ at $x = 0.2$ to $\Delta\varepsilon \sim 7-8$ at $x = 0.5$), which points to the enhancement of the corresponding magnetoelectric interaction.

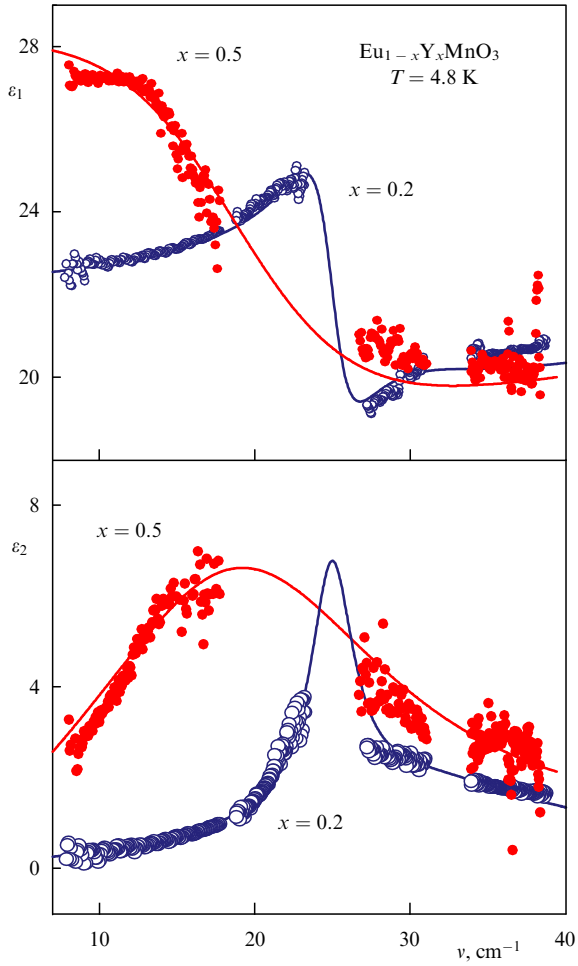

Figure 6. Electromagnon mode in the spectra of the real (ε_1) and imaginary (ε_2) parts of the dielectric constant $\varepsilon(\nu) = \varepsilon_1(\nu) + i\varepsilon_2(\nu)$ along the a-axis of the multiferroics $Eu_{1-x}Y_xMnO_3$ at $x = 0.2$ and 0.5 in the cycloidal ferroelectric phase. Points correspond to experimental data, and curves to calculated results.

Although no consistent microscopic theory for describing the mechanisms of the appearance of ferroelectricity and dynamic coupling in the multiferroics studied has yet been developed, it is already clear that the electric polarization vector appears as a result of breaking the centrosymmetricity of the system due to the appearance (in a specific temperature interval) of cycloidal magnetic structures incommensurate with the crystal lattice. At present, the most widely applied mechanism is the exchange-relativistic inhomogeneous magnetoelectric interaction which leads to the appearance of a local polarization vector $\mathbf{p} \sim \left[\mathbf{e}_{ij}[\mathbf{S}_i\mathbf{S}_j]\right]$ with a noncollinear arrangement of the adjacent spins, where $\mathbf{e}_{ij}$ is the vector that connects spins $\mathbf{S}_i$ and $\mathbf{S}_j$ [23, 25, 26] (Dzyaloshinskii–Moriya exchange interaction). The total polarization vector for this cycloidal structure proves to be proportional to the vector product of the wave vector $\mathbf{k}$ of the magnetic structure and the normal $\mathbf{e}$ to the plane of the spin rotation: $\mathbf{P} \sim [\mathbf{ek}]$ [23]. In the continuum approximation, as follows from a group-theoretical analysis, the observed ferroelectric properties of these multiferroics are caused by a Lifshitz type inhomogeneous magnetoelectric interaction:

$$\Phi_{\mathrm{me}} = -a_x P_x \left(A_x \frac{\partial A_y}{\partial y} - A_y \frac{\partial A_x}{\partial y} \right) - a_z P_z \left(A_z \frac{\partial A_y}{\partial y} - A_y \frac{\partial A_z}{\partial y} \right),$$

where $\mathbf{A}$ is the antiferromagnetic vector [12, 20], which both leads to a spontaneous polarization and determines the contribution to the dielectric constant and the coupling of the homogeneous electric field with spin excitations. With this type of magnetoelectric interaction, the change in the plane of rotation of Mn^{3+} spins in the cycloid from *bc* to *ab* should lead to a change in the excitation condition of electromagnons ($\mathbf{e} \| a \to \mathbf{e} \| c$); however, as follows from our and other investigations, this is not the case, and the electromagnons are observed only at the $\mathbf{e} \| a$ polarization. This means that another type of magnetoelectric coupling can also exist, which has been suggested recently in Ref. [22]. This type of magnetoelectric coupling, which has an exchange origin, is related to specific features of the crystal structure and determines the contribution to the dielectric constant along the *a*-axis irrespective of the cycloid orientation. However, as was revealed, this contribution comes only from high-lying spin excitations corresponding to the Brillouin zone boundary. Therefore, there is no full understanding of what role is played by the magnetoelectric interactions of this type in the formation of the electromagnon response, and the problem calls for additional investigations.

Acknowledgments

This work was supported in part by the Russian Foundation for Basic Research (project Nos 09-02-01355 and Bel_a-08-02-90060) and by the Program Kvantovaya Makrofizika (Quantum Macrophysics) of the Russian Academy of Sciences.

References

1. Fiebig M *J. Phys. D* **38** R123 (2005)
2. Tokura Y *Science* **312** 1481 (2006)
3. Cheong S-W, Mostovoy M *Nature Mater.* **6** 13 (2007)
4. Khomskii D I *J. Magn. Magn. Mater.* **306** 1 (2006)
5. Ramesh R, Spaldin N A *Nature Mater.* **6** 21 (2007)
6. Smolenskii G A, Chupis I E *Usp. Fiz. Nauk* **137** 415 (1982) [*Sov. Phys. Usp.* **25** 475 (1982)]
7. Kimura T et al. *Nature* **426** 55 (2003)
8. Goto T et al. *Phys. Rev. Lett.* **92** 257201 (2004)
9. Kimura T, Lashley J C, Ramirez A P *Phys. Rev. B* **73** 220401(R) (2006)
10. Kadomtseva A M et al. *Pis'ma Zh. Eksp. Teor. Fiz.* **81** 22 (2005) [*JETP Lett.* **81** 19 (2005)]
11. Kenzelmann M et al. *Phys. Rev. Lett.* **95** 087206 (2005)
12. Pimenov A et al. *Nature Phys.* **2** 97 (2006)
13. Sushkov A B et al. *Phys. Rev. Lett.* **98** 027202 (2007)
14. Aguilar R V et al. *Phys. Rev. B* **76** 060404(R) (2007)
15. Pimenov A et al. *Phys. Rev. B* **77** 014438 (2008)
16. Mukhin A A et al. *Izv. Ross. Akad. Nauk Ser. Fiz.* **71** 1658 (2007) [*Bull. Russ. Acad. Sci. Phys.* **71** 1617 (2007)]
17. Kida N et al. *Phys. Rev. B* **78** 104414 (2008)
18. Senff D et al. *Phys. Rev. Lett.* **98** 137206 (2007)
19. Senff D et al. *J. Phys. Condens. Matter* **20** 434212 (2008)
20. Pimenov A et al. *J. Phys. Condens. Matter* **20** 434209 (2008)
21. Takahashi Y et al. *Phys. Rev. Lett.* **101** 187201 (2008)
22. Aguilar R V et al. *Phys. Rev. Lett.* **102** 047203 (2009)
23. Mostovoy M *Phys. Rev. Lett.* **96** 067601 (2006)
24. Harris A B *Phys. Rev. B* **76** 054447 (2007)
25. Katsura H, Nagaosa N, Balatsky A V *Phys. Rev. Lett.* **95** 057205 (2005)
26. Sergienko I A, Dagotto E *Phys. Rev. B* **73** 094434 (2006)
27. Katsura H, Balatsky A V, Nagaosa N *Phys. Rev. Lett.* **98** 027203 (2007)
28. Chenglong Jia et al. *Phys. Rev. B* **76** 144424 (2007)
29. Ivanov V Yu et al. *J. Magn. Magn. Mater.* **300** e130 (2006)
30. Hemberger J et al. *Phys. Rev. B* **75** 035118 (2007)
31. Pimenov A et al. *Phys. Rev. Lett.* **102** 107203 (2009)
32. Volkov A A et al. *Infrared Phys.* **25** 369 (1985)
33. Kozlov G V, Volkov A A "Coherent source submillimeter wave spectroscopy", in *Millimeter and Submillimeter Wave Spectroscopy of Solids* (Ed. G Grüner) (Berlin: Springer, 1998) p. 51
34. Gorshunov B et al. *Int. J. Infrared Millimeter Waves* **26** 1217 (2005)

PACS numbers: **63.20.–e**, 68.35.Rh, **75.80.+q**, **77.55.+f**, **77.80.–e**
DOI: 10.3367/UFNe.0179.200908k.0909

Heteroepitaxial films of a bismuth ferrite multiferroic doped with neodymium

V M Mukhortov, Yu I Golovko, Yu I Yuzyuk

The possibility of the coexistence of spontaneous magnetic moments and electric polarization does not contradict the general criteria for the formation of ferromagnetism and ferroelectricity as separate phenomena. The magnetic ordering is determined by the exchange interaction of electron spins, while ferroelectric ordering by a redistribution of charge density in the crystal lattice. Bismuth ferrite ($BiFeO_3$) is one of the first ferroelectromagnets in which there were discovered ferroelectric [1, 2] and antiferromagnetic [3, 4] ordering with uniquely high temperatures of electric ($T_c = 1083$ K) and magnetic ($T_N = 643$ K) ordering, but the high electrical conductivity of the samples hampered their study and practical implementation [5].

At room temperature, the crystal structure of a bismuth ferrite single crystal is described by the space group *R*3*c*. Its rhombohedral unit cell ($a = 0.562$ nm, $\alpha = 59.35°$) contains two formula units. The spontaneous polarization is oriented in the direction [111] of the pseudocubic perovskite unit cell. G type antiferromagnetic ordering appears when the mag-

netic moments of iron ions, preserving a locally antiparallel orientation, are turned in a spiral oriented along the direction $[10\bar{1}]$. According to neutron-diffraction data [6], the period of this cycloid equals 62 nm. The interaction of spin waves with optical phonons in $BiFeO_3$ single crystals was recently investigated by light scattering methods [7].

Recently, interest in bismuth ferrite has grown sharply, which is connected with the detection in the films of this compound of a giant magnetoelectric (ME) effect (the appearance of magnetization under the action of an electric field [8]) and of a giant magnetocapacitance (the appearance of electric polarization under the action of a magnetic field [9]). Under normal conditions, these effects are not observed because of the presence of a cycloid — a spatially modulated structure in which the magnetization vectors of the sublattices periodically change direction from point to point. On account of the presence of a cycloid, the average-over-the-volume linear ME effect and spontaneous magnetization are equal to zero [10]. The magnetoelectric effect observed in $BiFeO_3$ films with a nanoscale thickness points to the destruction of the spatially modulated structure in films, which is caused by high internal deformation fields arising due to the misfit of the lattice parameters of the film and substrate and related deformation of the unit cell [11, 12]. As a result of electrostriction, these stresses in nanoscale films lead to the appearance of an additional contribution to the electric polarization. A similar effect occurs in ferroelastics. Therefore, the presence of magnetic ordering, a redistribution of charge density, and electrostriction lead to the appearance of new properties in heterostructures based on ferroelectromagnets (multiferroics, according to the contemporary terminology), which are quite important from the viewpoint of practical application.

Thus, the development of the methods of synthesis and crystallization of multiferroic heterostructures on different substrates has become an urgent task. For the real application of multiferroic films, it is necessary that the ferroelectric polarization, the piezoelectric coefficient, and the magnetization have sufficiently high values, just like the magnetoelectric interaction.

In recent years, new multiferroic materials with high values of physical characteristics have been obtained by doping traditional single-phase multiferroic $BiFeO_3$ with various ions of rare-earth metals [12, 13]. Doping with neodymium ions favors the suppression of the cycloidal structure and can lead to an increase in the remanent polarization and saturation magnetization [13], as well as to a decrease in the ferroelectric coercive field and leakage currents [12].

In this report, we present results on the preparation and investigation of heteroepitaxial films of $BiFeO_3$ multiferroic doped with neodymium and deposited on single-crystal MgO substrates.

To obtain the $(Bi_{0.98}Nd_{0.02})FeO_3$ (BNFO) films on (001) cuts of MgO single crystals, we used the technique of high-frequency (HF) sputtering of stoichiometric ceramic targets of the same composition at elevated pressures of oxygen, which earlier was successfully applied to obtaining epitaxial films of barium strontium titanate (BST) [14]. The basic distinction between our procedure of deposition and the known ones consisted in our using a heavy-current HF discharge to bring about film growth. The supplied high-frequency power (73 W cm^{-2}), a special geometry of the electrodes, and a high pressure of oxygen (0.6 Torr) made it possible to pulverize the oxide at a cluster level and to create in the plasma a dispersed phase of the initial oxide, which serves as a vapor phase for the growing film. The basic difference between the procedure of obtaining BST heterostructures and that of obtaining BNFO is in the effect of the substrate temperature on the synthesis and crystallization of the film. In the case of the BST structure, an increase in the temperature from 300 °C to 700 °C led to a progressive increase in the degree of structural perfection of the films in the following sequence: X-ray amorphous–polycrystalline–textured–single-crystalline, whereas in the structures on the base of BNFO the reverse sequence was observed as the substrate temperature increased from 340 °C to 550 °C: single-crystal films — textured films — polycrystalline films — films consisting of a mixture of oxides.

Measurements of the composition of the target and the films was performed using a Comebax-micro analyzer. As the standard, we used a $BiFeO_3$ single crystal. The neodymium concentration in the films coincided with the concentration in the target to an accuracy of 1%.

The structural perfection of the films, the lattice parameters along the normal to the substrate plane and in the substrate plane, and the orientation relationships between the film and the substrate at room temperature were established by X-ray diffraction method using a DRON-7 diffractometer ($\Theta-2\Theta$ method; taking symmetric and asymmetric Bragg reflections; Cu K_α radiation). The deposition of BNFO films on MgO (100) substrates showed that the threshold temperature of the substrate in the process of deposition for a single-crystal growth of the film runs to 350 °C, which is lower than the temperatures of both the ferroelectric and antiferromagnetic phase transitions. An increase in the temperature to above 500 °C leads to the film condensation in the form of a mixture of simple oxides.

The X-ray diffraction spectrum ($\Theta-2\Theta$ scanning) of a single-crystal BNFO film with a thickness of 35 nm on an MgO (100) substrate in the $20°-50°$ range of angles is given in Fig. 1. The diffractogram contains only (001) and (002) reflections of the perovskite phase of the BNFO, and a (002) reflection from the substrate, which indicates that the [001]-axis of the film is parallel to the [001]-axis of the MgO substrate. The vertical misorientation of the film relative to

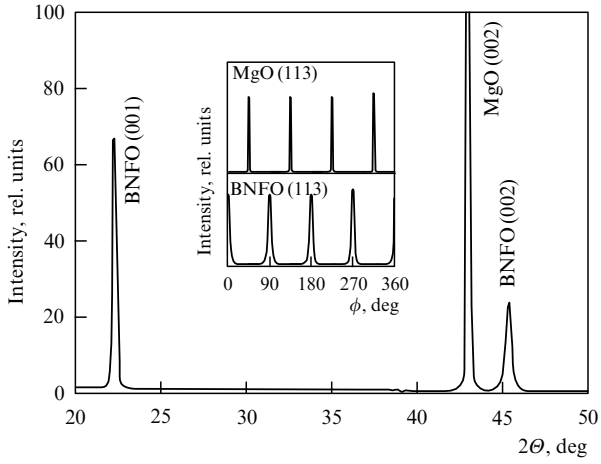

Figure 1. Typical X-ray diffraction pattern ($\Theta-2\Theta$ scanning) of a single-crystal BNFO film on MgO (001). The inset displays the diffractograms obtained by φ scanning of BNFO (113) and MgO (113) reflections.

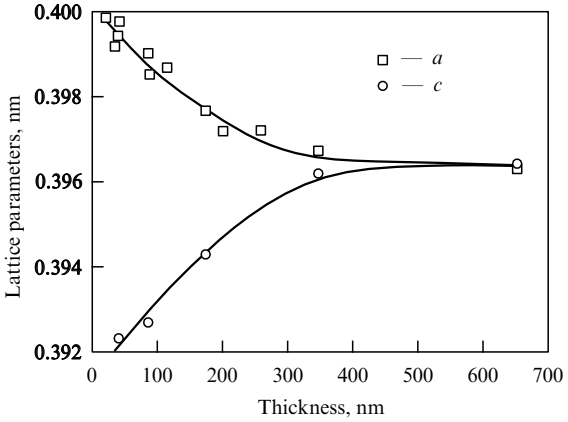

Figure 2. Variation of the lattice parameters along the normal to the film surface and in the film plane as a function of the film thickness.

the normal to the substrate, as determined from the widths of rocking curves, reaches $\sim 1^\circ$.

To prove the fact of heteroepitaxial growth, reveal the azimuthal misorientation of the film, and determine the orientation relationships between the film and substrate, we used the method of φ scanning of pseudocubic reflections (113) from the film and (113) reflections from the substrate. The corresponding X-ray diffractograms of (113) reflections from the film and the substrate are presented in the inset to Fig. 1. In the film, there is only one azimuthal orientation of the film relative to the substrate: the [001]-axis of the film is parallel to the [001]-axis of the MgO substrate, while the [100]- and [010]-axes of the film are oriented along the $[1\bar{1}0]$ and [110] directions of the substrate, respectively. Therefore, the diffractogram (see inset to Fig. 1) contains four reflections appearing when the sample is rotated in its plane through an angle of 360°, but the reflections from the film and substrate are shifted by an angle of 45° relative to each other.

To more precisely determine the lattice parameter c of the film in the direction of the normal to the film by the X-ray diffraction method, we used reflections of the $(00l)$ type. For determining lattice parameters of the film in the ab plane of the substrate, we used the asymmetric method of taking (024) type reflections. A room-temperature X-ray diffraction studies of BNFO films of different thicknesses on MgO (001) substrates revealed the presence of some peculiarities in the dependences of the film lattice parameters both along the normal to the plane of the substrate and in the plane of the substrate layer. The lattice parameters were calculated in the tetragonal approximation. As is shown in Fig. 2, in the region of thicknesses from 20 to 650 nm the lattice parameter c of the BNFO films along the normal to the plane of the base layer decreases, and the parameters in the substrate plane $a = b$ increase with increasing thickness of the film. In the region of small thicknesses, the lattice parameter c of the films is greater than the lattice parameter of the perovskite subcell of the rhombohedrally distorted phase of the bulk sample (0.3964 nm), whereas the parameter a is smaller, which testifies to the presence of compressive stresses in the films in the substrate plane. In the very thick BNFO films on MgO (001) substrates, the lattice parameters relax to values characteristic of the bulk state.

It should be noted here that in practice the MgO substrates (NaCl type structure, the lattice parameter $a = 0.4212$ nm) are mainly used to create tensile stresses in BST films, which has repeatedly been confirmed in works by various authors, as well as in ours. Taking into account the proximity of lattice parameters of the BST and BNFO films, this behavior of the lattice parameters of the BNFO films with decreasing thickness of the films can hardly be explained by the assumption about the prevailing influence of the misfit in the lattice parameters of the film and the substrate.

It is worthy of note that the epitaxial growth of perovskites on MgO (001) substrates was analyzed theoretically in Ref. [15], where it was shown that, from the viewpoint of the minimization of stresses and a considerable decrease in the density of misfit dislocations in the film, such a conjugation of the unit cells of the film and the substrate is energetically more advantageous where the unit cell of the film of the perovskite $PbTiO_3$ is rotated through 45° relative to that of MgO in the conjugation plane. However, in the case of films of the ferroelectric perovskite BST on MgO substrates, which were investigated in our previous work [14], the growth of the films always occurred with a parallel conjugation of the axes of the film and the substrate. The epitaxial growth with a turn of the crystallographic axes of the film relative to the MgO substrate is a specific feature of BNFO films, which still had to be clarified. No such conjugation effects were observed upon deposition of bismuth ferrite films on other substrates.

For the investigation of the dielectric characteristics of the films, planar electrodes were applied onto the film surface using contact photolithography and ion-beam sputtering of aluminium with a vanadium underlayer. The planar electrodes represented an interdigitated structure with aluminium electrodes about 0.3 μm thick. The interdigital planar capacitor consisted of 470 fingers with a dielectric clearance between them 0.65–0.75 μm wide at a length of 140 μm and width of 1.55–1.75 μm of each finger. The real geometrical dimensions of the planar capacitor for determining the dielectric constant after the lithographic process were obtained with a Leitz Latimet microscope. The capacity, conductivity, and leakage currents of the planar capacitors were measured with a Keithley 4200-SCS semiconductor characterization system at a frequency of 1 MHz with the aid of a PM-5 MicroTec probe station. The results of the measurements of the electrode topology and the capacity were used for calculating the dielectric constant according to the formulas given in Ref. [16].

In none of the samples investigated did the DC leakage currents exceed 10^{-9} A at an external voltage across the planar electrodes equal to 45 V, and the dielectric loss tangent at a frequency of 1 MHz was as low as 0.08. The dependence of the dielectric constant on the film thickness is presented in Fig. 3. In the inset to this figure, dielectric hysteresis loops are shown (at the film thickness of 70 nm), from which it is evident that at a frequency of 0.05 Hz the remanent electric polarization was 7 μC cm^{-2}; with increasing frequency, it decreased to 2 μC cm^{-2} at a frequency of 5 Hz and remained constant at frequencies of up to 10^3 Hz. The dielectric hysteresis loops obtained in our samples differ from those presented in Ref. [8] for films of the same composition, which even at high frequencies remain 'rectangular'. The dielectric hysteresis loops given in Ref. [12] occupy an intermediate position with respect to those considered above; however, in the last work the applied electric field was greater by an order of magnitude. It should be emphasized that the shapes of the dielectric hysteresis loops measured in the usual structure of a capacitor (metal–dielectric–metal) and with a planar struc-

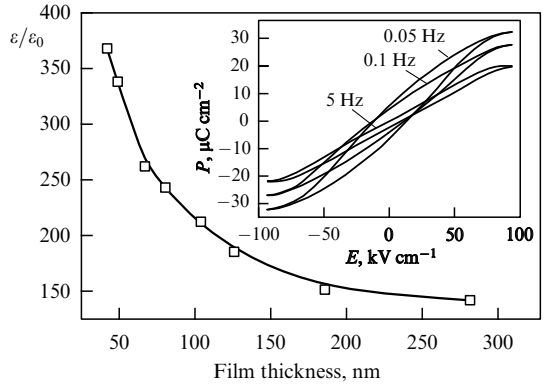

Figure 3. Effect of the thickness of a BNFO film on its dielectric constant. The inset shows dielectric hysteresis loops.

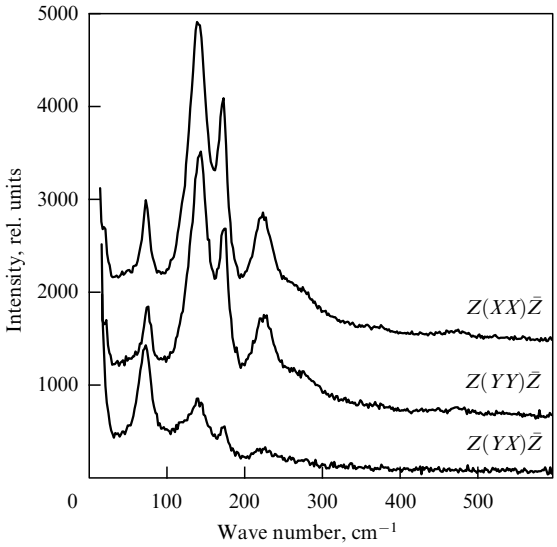

Figure 4. Polarized Raman spectra of a BNFO film in the geometries of normal backscattering.

ture of the electrodes should differ substantially as a result of the principally different field distribution. A study of the processes of polarization switching in planar capacitors is only beginning in essence, despite the fact that the practical employment of BNFO heterostructures on dielectric substrates is only possible with this topology of the electrodes.

The phonon spectra of the films were investigated by the Raman spectroscopy method. The spectra of micro-Raman scattering (MRS) were excited by polarized radiation from an argon laser ($\lambda = 514.5$ nm) and were detected by a Renishaw single-pass spectrometer equipped with a NExT (near-excitation tunable) filter for an analysis of the low-frequency region of the spectra. The exciting radiation was focused onto a sample using a Leica optical microscope; the diameter of the focused spot on the sample equaled 2 μm. The polarized Raman spectra were obtained in samples precisely oriented relative to the crystallographic axes of the MgO substrate. The coordinate system used was selected as follows: $X \parallel [100]$, $Y \parallel [010]$, and $Z \parallel [001]$.

The Raman spectra of the BNFO film (270 nm thick) obtained in the geometry of normal backscattering, in which the incident beam is directed along the normal to the film surface along the Z-axis, are given in Fig. 4. The polarized

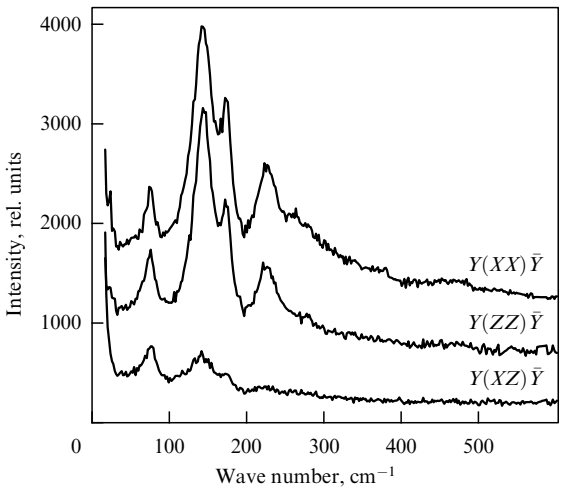

Figure 5. Polarized Raman spectra of a BNFO film in the geometries of backscattering from the butt edge of the film.

spectra of this film contain all the lines that were observed earlier in the spectra of bismuth ferrite single crystals at room temperature [17]. The unit cell of a rhombohedral single-crystal bismuth ferrite contains two formula units. The optical modes $4A_1 + 9E$ predicted by the factor-group analysis were identified in the spectra of a single crystal in Ref. [17]. Doping with neodymium does not virtually affect the phonon spectra.

No noticeable shifts in optical mode frequencies, indicating the presence of strong mechanical stresses in the film, have been observed in the spectra of a BNFO film. This is apparently explained by the above-described specific type of conjugation of the film with the crystal lattice of the MgO substrate. In the spectra of backscattering from the butt edge of the film given in Fig. 5, a line at 74 cm^{-1} is observed in the scattering geometry $Y(XZ)\overline{Y}$, originating from the E(TO) component of the soft mode, as are three intense lines at 142, 171, and 225 cm^{-1}, which originate from the A_1 symmetry modes of the rhombohedral phase of the $BiFeO_3$ single crystal [17]. The Raman spectra of the two diagonal orientations $[Y(XX)\overline{Y}$ and $Y(ZZ)\overline{Y}]$ are virtually equivalent, which also excludes the tetragonal c-domain structure of the film.

An important feature of the spectra of BNFO films on an MgO substrate is their electric polarization dependence, which has not been observed previously for films of pure or neodymium-doped bismuth ferrite. Thus, in the Raman spectra of polycrystalline rhombohedral BNFO films on the $Pt/TiO_2/SiO_2/Si$ substrates [12] and of films of pure $BiFeO_3$ on $LaNiO_3/SrTiO_3$ [18], no polarization dependence was observed because of the polycrystalline character of the films. The spectra of tetragonal c-domain $BiFeO_3$ films grown on $SrTiO_3$(001) substrates [19] were polarized in accordance with the selection rules for the tetragonal point group $P4mm$. Namely, in the scattering geometry $Y(XZ)\overline{Y}$ (the coordinate system coincides with that selected by us), modes of only E symmetry are observed. The Raman spectrum corresponding to the geometry $Z(YX)\overline{Z}$ contains only weak lines which appear from diagonal geometries because of polarization disturbances, whereas no intrinsic lines, corresponding to a given type of symmetry, have been revealed, which confirms the tetragonal symmetry of the film with a polarization direction along [001]-axis in the film grown on an $SrTiO_3$(001) substrate.

The polarization characteristics of the Raman spectra exclude the rhombohedral symmetry of the BNFO film on MgO. In addition, the presence of intense lines in the scattering geometry $Z(YX)\overline{Z}$ in our BNFO film unambiguously indicates that the film on an MgO substrate is not a tetragonal *c*-domain one. As is shown in Fig. 4, the low-frequency mode (72 cm^{-1}) in the geometry $Z(YX)\overline{Z}$ is almost twice as wide as the low-frequency peak in the $Z(YY)\overline{Z}$ spectrum, whose frequency amounts to 75 cm^{-1}. This fact testifies to the splitting of the E(TO) mode of the rhombohedral bismuth ferrite phase into two components manifesting themselves in different scattering geometries, which is possible only as a result of a reduction of the BNFO film symmetry to orthorhombic or even monoclinic. The spectra in the $Z(YY)\overline{Z}$ and $Z(XX)\overline{Z}$ geometries are virtually equivalent, and a rotation of the sample about the *Z*-axis through an angle of 45° does not affect the polarization characteristics of the spectra, which appears to be caused by a complex 90°-domain structure. The presence in the $Z(YX)\overline{Z}$ spectrum of an intense component of the soft mode suggests the orientation of the spontaneous electric polarization in the film plane or, at least, the presence of a polarization component that lies in this plane.

A symmetry analysis of structural distortions induced by the rotation of oxygen octahedra and by polar displacements of cations in films of perovskites obtained on cubic substrates was recently performed in Ref. [20], where more than 30 possible phases have been identified. To determine the symmetry of bismuth ferrite films doped with neodymium that are grown on MgO(001) single-crystal substrates, precision structural investigations are required. Since the destruction of a spin cycloid in the films can occur due to mechanical stresses, of special interest are investigations of films with different thicknesses.

References

1. Venevtsev Yu N, Zhdanov G S, Solov'ev S P *Kristallografiya* **5** 520 (1960)
2. Smolenskii G A et al. *Fiz. Tverd. Tela* **2** 2982 (1960) [*Sov. Phys. Solid State* **2** 2651 (1960)]
3. Smolenskii G A et al. *Zh. Eksp. Teor. Fiz.* **43** 877 (1962) [*Sov. Phys. JETP* **16** 622 (1963)]
4. Kiselev S V, Ozerov R P, Zhdanov G S *Dokl. Akad. Nauk SSSR* **145** 1255 (1962) [*Sov. Phys. Dokl.* **7** 742 (1963)]
5. Roginskaya Yu E et al. *Zh. Eksp. Teor. Fiz.* **50** 69 (1966) [*Sov. Phys. JETP* **23** 47 (1966)]
6. Sosnowska I, Neumaier T P, Steichele E *J. Phys. C* **15** 4835 (1982)
7. Cazayous M et al. *Phys. Rev. Lett.* **101** 037601 (2008)
8. Wang J et al. *Science* **299** 1719 (2003)
9. Kimura T et al. *Nature* **426** 55 (2003)
10. Kadomtseva A M et al. *Pis'ma Zh. Eksp. Teor. Fiz.* **79** 705 (2004) [*JETP Lett.* **79** 571 (2004)]
11. Zvezdin A K, Pyatakov A P *Usp. Fiz. Nauk* **174** 465 (2004) [*Phys. Usp.* **47** 416 (2004)]
12. Yuan G L et al. *J. Appl. Phys.* **101** 024106 (2007)
13. Huang F et al. *Appl. Phys. Lett.* **89** 242914 (2006)
14. Mukhortov V M, Yuzyuk Yu I *Geterostruktury na Osnove Nanorazmernykh Segnetoelektricheskikh Plenok: Poluchenie, Svoistva i Primenenie* (Heterostructures on the Base of Nanoscale Ferroelectric Films: Preparation, Properties, and Applications) (Rostov-on-Don: Izd. YuNTs RAN, 2008)
15. Lahoche L et al. *J. Appl. Phys.* **91** 4973 (2002)
16. Vendik O G, Zubko S P, Nikol'skii M A *Zh. Tekh. Fiz.* **69** (4) 1 (1999) [*Tech. Phys.* **44** 349 (1999)]
17. Fukumura H et al. *J. Magn. Magn. Mater.* **310** e367 (2007)
18. Yang Y et al. *J. Appl. Phys.* **103** 093532 (2008)
19. Singh M K, Ryu S, Jang H M *Phys. Rev. B* **72** 132101 (2005)
20. Shirokov V B, Yuzyuk Yu I, Lemanov V V *Fiz. Tverd. Tela* **51** 972 (2009) [*Phys. Solid State* **51** 1025 (2009)]